Biomaterials 280 (2022) 121258

Contents lists available at ScienceDirect

Biomaterials

journal homepage: www.elsevier.com/locate/biomaterials

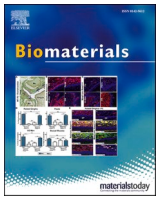

A multivalent Ara-C-prodrug nanoconjugate achieves selective ablation of leukemic cells in an acute myeloid leukemia mouse model

Victor Pallarès [a,b,c,1], Ugutz Unzueta [a,b,c,f,1], Aïda Falgàs [a,b,c,1], Anna Aviñó [c,d], Yáiza Núñez [a,b], Annabel García-León [a,b], Laura Sánchez-García [c,e,f], Naroa Serna [c,e,f], Alberto Gallardo [a,g], Lorena Alba-Castellón [a,b], Patricia Álamo [a,b,c], Jorge Sierra [b,h], Lídia Cedó [a,i], Ramon Eritja [c,d], Antonio Villaverde [c,e,f], Esther Vázquez [c,e,f,***], Isolda Casanova [a,b,c,**], Ramon Mangues [a,b,c,*]

[a] Biomedical Research Institute Sant Pau (IIB Sant Pau), Barcelona, 08041, Spain
[b] Josep Carreras Leukaemia Research Institute, Barcelona, 08916, Spain
[c] CIBER en Bioingeniería, Biomateriales y Nanomedicina (CIBER-BBN), Madrid, 28029, Spain
[d] Institute for Advanced Chemistry of Catalonia (IQAC), CSIC, Barcelona, 08034, Spain
[e] Institute of Biotechnology and Biomedicine (IBB), Universitat Autònoma de Barcelona, Bellaterra, 08193, Spain
[f] Department of Genetics and Microbiology, Universitat Autònoma de Barcelona, Bellaterra, 08193, Spain
[g] Department of Pathology, Hospital de la Santa Creu i Sant Pau, Barcelona, 08025, Spain
[h] Department of Hematology, Hospital de la Santa Creu i Sant Pau, Barcelona, 08025, Spain
[i] CIBER de Diabetes y Enfermedades Metabólicas Asociadas (CIBERDEM), Madrid, 28029, Spain

ARTICLE INFO

Keywords:
Targeted protein nanoparticle
Multivalency
Targeted drug delivery
Ara-C prodrug
CXCR4
Acute myeloid leukemia

ABSTRACT

Current therapy in acute myeloid leukemia (AML) is based on chemotherapeutic drugs administered at high doses, lacking targeting selectivity and displaying poor therapeutic index because of severe adverse effects. Here, we develop a novel nanoconjugate that combines a self-assembled, multivalent protein nanoparticle, targeting the CXCR4 receptor, with an Oligo-Ara-C prodrug, a pentameric form of Ara-C, to highly increase the delivered payload to target cells. This 13.4 nm T22-GFP-H6-Ara-C nanoconjugate selectively eliminates $CXCR4^+$ AML cells, which are protected by its anchoring to the bone marrow (BM) niche, being involved in AML progression and chemotherapy resistance. This nanoconjugate shows CXCR4-dependent internalization and antineoplastic activity in $CXCR4^+$ AML cells in vitro. Moreover, repeated T22-GFP-H6-Ara-C administration selectively eliminates $CXCR4^+$ leukemic cells in BM, spleen and liver. The leukemic dissemination blockage induced by T22-GFP-H6-Ara-C is significantly more potent than buffer or Oligo-Ara-C-treated mice, showing no associated on-target or off-target toxicity and, therefore, reaching a highly therapeutic window. In conclusion, T22-GFP-H6-Ara-C exploits its 11 ligands-multivalency to enhance target selectivity, while the Oligo-Ara-C prodrug multimeric form increases 5-fold its payload. This feature combination offers an alternative nanomedicine with higher activity and greater tolerability than current intensive or non-intensive chemotherapy for AML patients.

1. Introduction

Over the last four decades, the 7 + 3 remission induction therapy has been the standard of care for acute myeloid leukemia (AML). This intensive chemotherapy treatment is based on the use of high doses of Ara-C (cytosine arabinoside; cytarabine) combined with anthracyclines, usually daunorubicin or idarubicin [1,2]. In most patients, this therapy is able to eliminate leukemic cells achieving a complete remission, but fatally killing normal hematopoietic cells, which, in turn, may put the patient at risk of suffering complications such as infections,

* Corresponding author. Biomedical Research Institute Sant Pau (IIB-Sant Pau), Josep Carreras Leukaemia Research Institute (IJC) and CIBER-BBN, Spain.
** Corresponding author. Biomedical Research Institute Sant Pau (IIB-Sant Pau), Josep Carreras Leukaemia Research Institute (IJC) and CIBER-BBN, Spain.
*** Corresponding author. Institute of Biotechnology and Biomedicine (IBB) and Department of Genetics and Microbiology, Universitat Autònoma de Barcelona and CIBER-BBN, Spain.
E-mail addresses: esther.vazquez@uab.cat (E. Vázquez), icasanova@santpau.cat (I. Casanova), rmangues@santpau.cat (R. Mangues).
[1] VP, UU and AF contributed equally to this work.

https://doi.org/10.1016/j.biomaterials.2021.121258
Received 26 May 2021; Received in revised form 22 October 2021; Accepted 13 November 2021
Available online 24 November 2021

inflammatory processes, cardiotoxicity or even death [3–5]. In addition, other patients, specially the elderly or those with unfavorable profiles, cannot be considered candidates for intensive chemotherapy [1].

In recent years, novel therapies have been approved by the FDA to treat patients with specific molecular alterations, for instance, FLT3 or IDH inhibitors, antibody drug conjugates targeting overexpressed CD33 or CD123 surface receptors, or inhibitors of proteins that regulate leukemic cell survival or proliferation pathways, such as BCL or Hedgehog [6–9]. However, most of these drugs are small molecules that use passive diffusion, have a short half-life in blood, undergo renal clearance and do not efficiently accumulate in tumors [10–12]. Therefore, new specific targeted drugs that overcome these limitations, and consequently increase antineoplastic efficacy while reducing systemic toxicity, are still needed. To this purpose, nanomedicines can become a new tool to improve the pharmacokinetic properties and the biodistribution of classical drugs by selectively delivering potent cytotoxic drugs directly to leukemic cells exploiting the receptor overexpression observed in malignant cells [13–15]. In fact, we have designed a multivalent nanoparticle capable of selective internalization in leukemic cells that overexpress the receptor CXCR4 [16]. CXCR4 is a chemokine receptor that is overexpressed in leukemic cells in a large number of AML patients, conferring a poor prognosis or higher relapse rate to them [17–22]. In addition, CXCR4 and its SDF1 ligand are determinants of minimal residual disease (MRD) and limit chemotherapy effectiveness in AML patients [23,24]. T22-GFP-H6 is a self-assembled protein nanoparticle that incorporates around 11 T22 peptidic ligands, acquiring multivalency for CXCR4 binding. This property confers the nanoparticle the capacity to selectively internalize in CXCR4-overexpressing ($CXCR4^+$) leukemic cells. In fact, we have previously demonstrated the ability of this nanoparticle, once conjugated to a microtubule inhibitor, to internalize and eliminate target leukemic cells [25]. Here, we demonstrate that the conjugation of the multivalent T22-GFP-H6 nanoparticle to a new prodrug, a pentameric form of Ara-C, accommodates a high payload of this drug, which is used in standard care of several hematological cancers. Thus, the use of T22-GFP-H6-Ara-C could be more effective than equimolar doses of Oligo-Ara-C in a disseminated $CXCR4^+$ AML mouse model.

2. Material and methods

2.1. Cell lines

THP-1 and SKM-1 AML cell lines were purchased from DSMZ (Leibniz Institute DSMZ-German Collection of Microorganisms and Cell Cultures, Braunschweig, Germany). Cells were cultured in RPMI-1640 medium supplemented with 10% FBS, 10 mmol/L L-glutamine, 100 U/mL penicillin, 10 mg/mL streptomycin and 0.45 μg/mL fungizone (Gibco, Thermo Fisher Scientific (TFS), Waltham, MA, US) and kept at 37 °C in a humidified atmosphere of 5% CO_2. Furthermore, THP-1 cells were transfected with a plasmid encoding the luciferase gene using Lipofectamine LTX and PLUS reagents (A12621, Invitrogen, TFS) according to the manufacturer's instructions which conferred bioluminescence (BLI) to the cells (hereinafter referred to as THP-1-Luci).

2.2. Protein nanoparticles production and purification

Synthetic gene encoding for T22-GFP-H6 protein was designed in house and provided by Geneart (Thermo Fisher) into pET22b plasmid (Novagen). T22-GFP-H6 nanoparticles were produced in *E.coli* Origami B (Novagen) O/N at 20 °C upon induction with 0.1 mM IPTG (isopropyl-β-D-thiogalactopyronaside). Cells were then harvested by centrifugation (15 min at 5000 g) and disrupted in a Tris buffer (20 mM Tris, 500 mM NaCl, 10 mM Imidazole) supplemented with EDTA-Free protease inhibitor cocktail (cOmplete™ EDTA-Free, Roche Diagnostics, Basel, Switzerland) by 3 rounds of French press (Thermo) at 1200 psi. Protein containing soluble fraction was then separated by centrifugation (45 min at 20,000 g) and charged in a HiTrap Chelating HP 1 mL column (GE Healthcare) for IMAC protein purification with an ÄKTA pure (GE Healthcare). Protein elution was performed by a lineal gradient of elution buffer (20 mM Tris, 500 mM NaCl, 500 mM Imidazole) and purified protein fraction was then dialyzed against sodium carbonate with salt buffer (166 mM $NaCO_3H$, 333 mM NaCl pH = 8). Protein purity was determined by SDS-PAGE electrophoresis followed by western-blot immunodetection with an anti-His monoclonal antibody (Santa Cruz Biotechnology) and protein integrity was determined by MALDI-TOF mass spectrometry. Purified protein nanoparticles amount was finally determined by Bradford assay.

2.3. T22-GFP-H6-Ara-C conjugation

Oligonucleotides containing Ara-C (Oligo-Ara-C) were prepared using the commercial protected N^4-Acetyl-2′-O-acetyl-5′-O-DMT-arabinosyl cytosine 3′-CE phosphoramidite unit (Carbosynth) following standard methodologies (Supporting Information and Fig. S1). T22-GFP-H6-Ara-C nanoconjugates (NCs) were generated by covalent binding of T22-GFP-H6 nanoparticles and Oligo-Ara-C (Ara-C pentameric form) through protein lysine amines in a two-step reaction. For that, thiol functionalized Oligo-Ara-C molecules were first separated from DTT by NAP-10 sephadex desalting column (GE Healthcare) and then reacted with an EMCS bi-functional cross-linker (6-Maleimidohexanoic acid *N*-hydroxysuccinimide ester) by thiol-Maleimide reaction in a 1:1 (Oligo-Ara-C: linker) molar ratio for 10 min at R.T. This reaction efficiently incorporates active NHS-ester groups to Oligo-Ara-C. NHS-ester functionalized Oligo-Ara-C molecules were then immediately reacted with T22-GFP-H6 external lysine-amines at a 1:5 (protein:Oligo-Ara-C) molar ratio O/N at R.T. Generated NCs were finally dialyzed against sodium carbonate with salt buffer in a high permeability 12–14 MWCO membrane (Spectrum labs) in order to remove non-reacted free Oligo-Ara-C molecules. Generation of NCs was determined by MALDI-TOF mass spectrometry, and conjugated Oligo-Ara-C amount was finally quantified by UV/visible light spectrophotometry at 260 nm.

2.4. Light scattering analysis

Volume size distribution and zeta potential of T22-GFP-H6 nanoparticles and T22-GFP-H6-Ara-C NCs were determined by Dynamic Light Scattering (DLS) and Electrophoretic Light Scattering (ELS) respectively at 633 nm in a Zetasizer Nano ZS (Malvern instruments). Samples were measured in triplicate and average peak size (nm), zeta (mV) and polydispersion index (pdi) were calculated.

2.5. Electron microscopy

Ultrastructural morphology (size and shape) of T22-GFP-H6-Ara-C nanoconstructs was visualized with two rapid high-resolution imaging techniques. Drops of 5 μL of sample diluted at 0.2 μg/mL in its buffer were deposited both in silicon wafers (Ted Pella) for field emission scanning electron microscopy (FESEM) and negatively stained with 2% uranyl acetate (Merck) in 400 mesh carbon-coated copper grids (Electron Microscopy Sciences) for transmission electron microscopy (TEM). Images of general fields and nanoparticle details were obtained at three magnifications with a FESEM Merlin (Zeiss) operating at 1 kV and equipped with an *in-lens* secondary electron detector and a TEM JEM 1400 (Jeol) operating at 80 kV and equipped with an Orius SC200 CCD camera (Gatan), respectively.

2.6. Fluorescence determination

Fluorescence of T22-GFP-H6 nanoparticles and T22-GFP-H6-Ara-C NCs was measured in a Varian Cary Eclipse fluorescence spectrophotometer (Agilent Technologies) upon excitation at 450 nm and emission scan from 500 to 525 nm. Samples were measured in triplicate.

2.7. Confocal laser microscopy

THP-1 cells were cultured in 24 well plates and incubated with 1 μM T22-GFP-H6-Ara-C or buffer for 2 h to evaluate NC internalization by confocal microscopy. Cell nuclei and membranes were then labeled with 0.2 μg/mL Hoechst 33 342 (Molecular Probes) and 2.5 μg/mL CellMask Deep Red (Molecular Probes) respectively for 10 min and subsequently washed in DPBS (Gibco) twice before adding fresh medium. Cells were finally transferred to a slide, covered by a glass cover and recorded in a TCS-SP5 confocal laser scanning microscope (Leica Microsystems) using a Plan Apo 63 x/1.4 (oil HC x PL APO lambda blue) objective and a blue diode (405 nm), an Ar laser (488 nm) and a HeNe laser (633 nm) for Hoechst, GFP and CellMask excitation respectively. Z stacks of different sections were also acquired every 0.5 μm and 3D images analyzed using Imaris 7.2.1 software (Bitplane).

2.8. Internalization and antineoplastic capacities of T22-GFP-H6-Ara-C in CXCR4$^+$ AML cell lines

First, the internalization capacity of the T22-GFP-H6-Ara-C was evaluated in AML cells. THP-1 and SKM-1 were cultured at 20×10^4 cells/mL and were treated with the NC at 50, 125 and 250 nM for 1 or 24 h. After that, cells were washed with PBS and were treated with Trypsin-EDTA (0.5%, no phenol red, Gibco, TFS) at 1 mg/mL for 15 min to remove the membrane-bound NCs that were not internalized. After 2 washes with PBS, GFP fluorescence was measured by flow cytometry using FACS Calibur cytometer. Two technical and biological replicates were performed for each condition. Data acquisition was analyzed by Cell Quest Pro software and results were expressed as mean fluorescence intensity (MFI) relative to the MFI of the buffer (MFIR) ± standard error (SE).

Secondly, a receptor competition assay was performed pre-treating or not THP-1 cells with AMD3100, an antagonist of CXCR4, at 7500 nM for 1 h prior to the exposure to 250 nM of T22-GFP-H6-Ara-C (ratio 30:1) for 1, 24 or 48 h. Trypsin-EDTA incubation and FACS analyses were performed as described above and results were presented as percentage of cells with T22-GFP-H6-Ara-C internalization after exposed them with AMD3100 compared with the group of cells exposed to NC without AMD3100.

Finally, T22-GFP-H6-Ara-C antineoplastic activity was evaluated in CXCR4$^+$ AML cell lines and compared with the Oligo-Ara-C anticancer activity at equimolar doses. THP-1 and SKM-1 were cultured at 30×10^4 cells/mL and treated with T22-GFP-H6-Ara-C or Oligo-Ara-C at different concentrations between 25 and 500 nM (equimolar doses for Oligo-Ara-C between 91.5 and 1830 nM) for 48 h. Then, cells were incubated for 4 h with the XTT reagents (Cell Proliferation Kit II, Roche Diagnostics) and the absorbance was measured at 492 nm in a FLUOstar OPTIMA spectrophotometer (BMG Labtech, Ortenberg, Germany). Cell viability percentage was obtained by subtracting the absorbance of the blanks and expressing each condition as percentage of cell growth (±standard error, SE), as compared with untreated controls (buffer treated cells). Five technical and three biological replicates were performed for each condition.

2.9. T22-GFP-H6-Ara-C pharmacokinetics and biodistribution in a subcutaneous (SC) AML mouse model

Four-week old female Swiss Nude mice were obtained from Charles River Laboratories (Wilmington, MA, US). Mice were maintained in specific pathogen-free (SPF) conditions with sterile food and water ad libitum. All in vivo procedures were conducted in accordance with the guidelines approved by the institutional animal Ethics Committee of Hospital Sant Pau (project number 10108 by the Government of Catalonia) and performed following the European Union Directive 2010–63-EU for welfare of the laboratory animals.

After 1 week of quarantine, 10 million THP-1 cells were injected subcutaneously in a single dorsal flank of each mice. Tumor growth was monitored twice a week with a caliper (tumor volume = width^2 x length/2). When tumors reached a volume of 300–500 mm^3, control mice ("Buffer") received a single intravenous dose of NC buffer ($NaCO_3H$ NaCl pH = 8, n = 3) whereas experimental mice ("T22-GFP-Ara-C") an intravenous dose of 200 μg T22-GFP-H6-Ara-C, which contains the GFP fluorescent protein that allows the in vivo NC tracking. Experimental mice were euthanized at different time points (10 min, 30 min, 2 h, 5 h, 24 h and 48 h, n = 3/group) after the NC administration. The ex vivo fluorescence intensity (FLI) was quantified in SC tumors, spleen, liver, heart, lungs, backbone, brain and plasma. Plasma was obtained by intracardiac puncture (25G) and blood centrifugation at 600*g* for 10 min at 4 °C. Moreover, we also collected urine from control and experimental mice.

The emitted FLI was registered with the IVIS Spectrum (124 262, PerkinElmer, Waltham, MA, USA). FLI correlates to the amount of accumulated protein in each tissue and is expressed as average radiant efficiency. FLI from experimental mice was calculated subtracting the FLI auto-fluorescence of control mice. Finally, the T22-GFP-H6-Ara-C biodistribution in all organs from 2 to 48 h was measured by cumulative FLI using the area under the curve (AUC).

2.10. Detection of T22-GFP-H6-Ara-C in plasma and urine by western blot

The same volume of plasma (2 μL) or urine (10 μL) from mice treated with buffer or T22-GFP-H6-Ara-C at different time points were used for the NC detection. The rest of volume until 20 μL was added with Milli-Q water and 4 μL of LB6X-DTT 3 M was mixed to each sample. Then, samples were separated using 15% SDS-PAGE and transferred to a nitrocellulose blotting membrane. Membranes were blocked with 5% skim milk in TBST for 2 h at room temperature, and then incubated with the 1:500 GFP primary antibody (sc-9996, Santa Cruz Biotechnology) O/N. Membranes were washed with TBST and then incubated with the mouse secondary antibody (1:10 000, Jackson Immune Research, West Grove, Pennsylvania, USA) for 1 h. The positive control for GFP detection was 1 ng of T22-GFP-H6-Ara-C. Western blot visualization was performed using the SuperSignal West Pico Chemiluminescent Substrate (Thermo Fisher Scientific) and the Universal Hood II Gel Doc Imaging System (BioRad).

2.11. Evaluation of the in vivo antineoplastic effect of T22-GFP-H6-Ara-C in a CXCR4$^+$ AML mouse model

To assess the antineoplastic activity of T22-GFP-H6-Ara-C in vivo, a CXCR4$^+$ AML disseminated mouse model was used [25].

NSG (NOD-*scid* IL2Rgamma^{null}) female mice (4 weeks old) were obtained from Charles River Laboratories and housed in microisolator units with sterile food and water ad libitum. In a preliminary assay, we run an experiment to identify the most effective anticancer dosage in vivo that showed no toxicity. After one week of quarantine, twenty NSG mice were intravenously (i.v.) injected with THP-1-Luci cells (1×10^6 cells/200 μL) and randomized into a control group and four different experimental groups (n = 4/group). Two days later, mice were i.v. daily injected with NC buffer ($NaCO_3H$ NaCl pH = 8) in the control group, and the other four groups with daily doses of 5, 25, 100 or 200 μg of T22-GFP-H6-Ara-C for 10 days. The AML progression in the mice was monitored every 2 or 3 days in IVIS Spectrum by detecting in vivo BLI in mice. Weight of mice was controlled during the experiment and all of them were euthanized the first day at which any mouse presented relevant signs of disease such as lack of mobility or 10% weight loss.

Afterwards, a more exhaustive study with a higher number of mice was performed with the most effective T22-GFP-H6-Ara-C dosage that lacks off-target toxicity (200 μg, n = 8) compared to mice treated with the Oligo-Ara-C at an equimolar dose (23.85 nmol, n = 8) and the NC buffer ($NaCO_3H$ NaCl pH = 8, n = 8) (Fig. S2A). Following the

experimental design from the previous experiment, each treatment was administered for 10 daily doses and the AML mouse progression as well as mouse weight were also registered every 2 or 3 days. BLI of relevant organs and tissues such as spleen, liver, hindlimbs, cranium and backbone were analyzed ex vivo after euthanasia. Then, tissues were fixed in formaldehyde 3.7% and paraffin-embedded for further histological and immunohistochemistry analyses. Results were expressed as Total flux of BLI (photons/second; Radiance photons) ± SE for the in vivo studies and as Average Radiance of BLI (photons/second/cm^2/sr) ± SE for the ex vivo studies.

2.12. Hepatic and renal function for toxicity assessment

Blood samples were collected from the in vivo preliminary assay (mice treated with buffer or 5, 25, 100 or 200 μg of T22-GFP-H6-Ara-C for a total of 10 doses, n = 4/group) at the last day (day 14) after intracardiac puncture (25G). Plasma of each mouse was obtained by centrifugation of total blood at 600 g for 10 min (min) at 4 °C. Aspartate transaminase (AST) and alanine transaminase (ALT) enzyme activities for the hepatic toxicity and creatinine levels for renal toxicity were determined using commercial kits (ASTL ref. 20764949 322; ALTL ref. 20764957 322 and CREJ2 ref. 04810716 190, Roche Diagnostics) and adapted for a COBAS 6000 autoanalyzer (Roche Diagnostics).

2.13. Histological and immunohistochemical staining

Detection of leukemic cells in the disseminated AML mice, treated with T22-GFP-H6-Ara-C, Oligo-Ara-C or buffer, was performed by immunohistochemistry (IHC) using the anti-human CD45 antibody (IR75161-2, Agilent, Dako) to stain only the leukemic THP-1-Luci cells in tissues such as liver, spleen, backbone and hindlimbs. Dako Autostainer Link 48 was used to perform this IHC staining following the manufacturer's instructions. Leukemic cell infiltration was evaluated and quantified using an Olympus BX53 microscope (Olympus, Tokyo, Japan) and the cellSens Dimension software (Olympus) using the Counter and Measurement tool choosing 4 fields randomly for each tissue. Results were presented as percentage of stained area ±SE. Images were acquired using an Olympus DP73 digital camera and processed with cellSens Dimension 1.9 software (Olympus). All samples were evaluated by two independent observers with an inter-observer agreement of 95%.

To analyze the potential toxicity of treatments in tissues, hematoxylin and eosin staining was performed in lung, kidney, liver, heart, backbone, hindlimbs and spleen. Two independent observers and an expert pathologist evaluated the possible toxicity in non-leukemic cells of these tissues using the Olympus BX53 microscope (Olympus).

2.14. Statistical analysis

Statistical analyses were performed in the IBM SPSS Statistics (Release 25.0, New York, NY, USA). Mann-Whitney *U* test was used in both in vitro and in vivo assays, and any differences were considered statistically significant when the *p-value* was lower than 0.05. $p < 0.05$ and $p < 0.01$ were indicated in figures and graphs by * or **, respectively. AUC analyses were performed with GraphPad Prism software (Version 6.01, GraphPad Software, Inc., San Diego, CA, USA). IC_{50} was calculated with SigmaPlot (Release 12.0.0.182; Systat Software, Inc., San Jose, CA, USA) using non-linear regression test with Hill-4 parameter adjustment.

3. Results

3.1. Characterization and synthesis of T22-GFP-H6-Ara-C NCs

In order to generate T22-GFP-H6-Ara-C NCs, a two-step reaction was used for the covalent binding of prior synthetized pentameric oligonucleotides of Ara-C (Oligo-Ara-C) (Supporting Information and Fig. S1) to the T22-GFP-H6 targeting vector (Fig. 1A). First, a 6-Maleimidohexanoic acid N-hydroxysuccinimide ester (EMCS) bifunctional crosslinker was covalently bound to a thiol functionalized Oligo-Ara-C (Oligo-Ara-C-SH) by maleimide-thiol reaction, generating a thioester bond. Then, the generated Oligo-Ara-C-Linker complexes were subsequently reacted with T22-GFP-H6 protein through exposed lysine-amines by NHS ester-amino reaction generating an amide bond.

This process resulted in the efficient binding of an average of 3–4 pentameric Oligo-Ara-C molecules per protein, that was calculated by UV light spectrophotometry and further corroborated by MALDI-TOF mass spectrometry. In concordance with the spectrophotometry data, T22-GFP-H6-Ara-C NCs showed up to four additional peaks with sequential molecular weight (MW) increase of around 2172 Da (range: 2138–2242 Da) over the MW of T22-GFP-H6 (30.6 kDa) in its MALDI-TOF spectrum (Fig. 1B). Each of those peaks correspond to the addition of an increasing number of Oligo-Ara-C (calculated MW:2271 Da) molecules per proteins.

Volume size distribution analysis showed low but significant differences between T22-GFP-H6 nanoparticles and T22-GFP-H6-Ara-C NCs size. DLS assays determined that the size of T22-GFP-H6 was 12.2 ± 0.2 nm, whereas the NC size was 13.4 ± 0.2 nm. In addition, the incorporation of negatively charged Oligo-Ara-C nucleotides to the protein resulted in a significant increase in the negative charge of T22-GFP-H6-Ara-C NCs compared to the unconjugated T22-GFP-H6 (zeta potential: −12.1 ± 0.6 *vs* −9.7 ± 0.5 mV, respectively) (Fig. 1C). Transmission Electron Microscopy (TEM) and Field Emission Scanning Electron Microscopy (FESEM) images revealed pseudoespherical NCs that validated the size determined by DLS (Fig. 1D). Furthermore, the fluorimetry assay showed no significant differences in the specific fluorescence levels between the conjugated and unconjugated nanoparticles (Fig. 1E). Finally, the incubation of T22-GFP-H6-Ara-C with CXCR4$^+$ THP-1 cells resulted in the intracellular localization of the NCs as determined by confocal laser microscopy (Fig. 1F).

3.2. Internalization capacity of T22-GFP-H6-Ara-C and competition with AMD3100 in CXCR4$^+$ AML cell lines

First, in order to evaluate the capacity of T22-GFP-H6-Ara-C NCs to internalize into leukemic cells through the CXCR4 receptor, we used two AML cell lines, THP-1 and SKM-1, that present high CXCR4 levels in their surface, which we have reported in a previous work [25]. Flow cytometry assays showed that T22-GFP-H6-Ara-C internalized in both CXCR4$^+$ leukemic cell lines (THP-1 and SKM-1) in a dose-dependent manner after 1 h exposure to the NC. Twenty-four hours later, the NC internalization increased significantly at 125 and 250 nM in both cell lines (Fig. 2A and B). Moreover, we analyzed if the internalization was dependent on the CXCR4 receptor by performing competition assays with the antagonist of CXCR4 AMD3100. T22-GFP-H6-Ara-C internalization was reduced significantly, in the range of 60–80%, at 1, 24 and 48 h after NC exposure and 1 h pre-treatment with AMD3100 (Fig. 2C).

3.3. Antineoplastic effect of T22-GFP-H6-Ara-C in CXCR4$^+$ AML cell lines

Afterwards, we analyzed the antineoplastic activity of T22-GFP-H6-Ara-C in THP-1 and SKM-1 cell lines. Exposure to T22-GFP-H6-Ara-C showed a dose-dependent antineoplastic effect in THP-1 and SKM-1 cells (Fig. 2D and E). IC_{50} of T22-GFP-H6-Ara-C was calculated for both cell lines. In THP-1, the IC_{50} was 108 ± 35 nM, whereas in SKM-1 was 78 ± 7 nM. No significant differences in anticancer activity were found between both lines, either when considering specific concentrations or when comparing THP-1 and SKM-1 IC_{50} values.

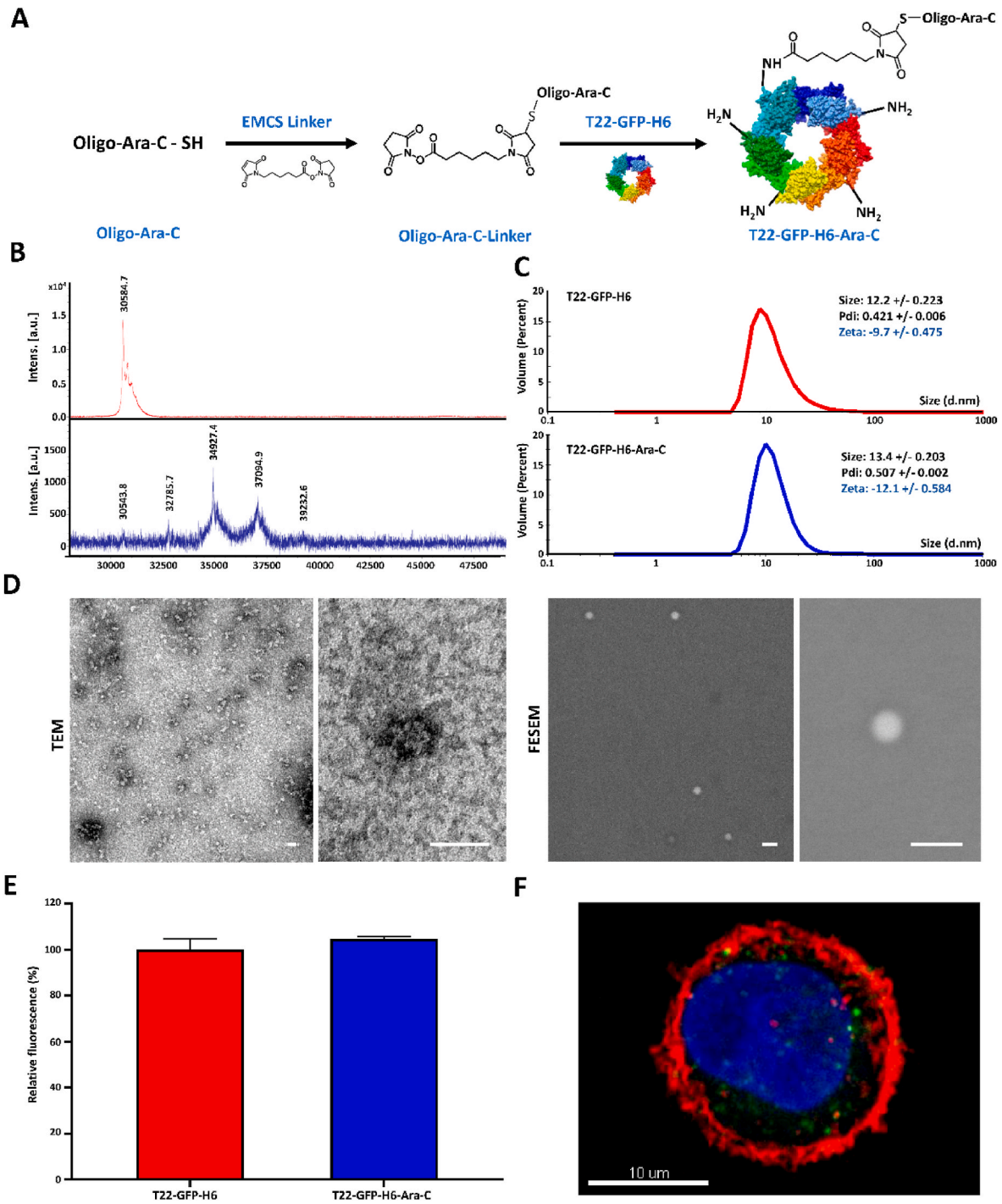

Fig. 1. Physicochemical characterization of T22-GFP-H6-Ara-C NCs. (A) Schematic representation of the two-step chemical Oligo-Ara-C conjugation to T22-GFP-H6 nanoparticles through protein lysine-amines by a bifunctional EMCS crosslinker. (B) MALDI-TOF mass spectrometry of T22-GFP-H6 nanoparticles (top) and T22-GFP-H6-Ara-C NCs (bottom). Each peak over 30.6 kDa in T22-GFP-H6-Ara-C indicates the incorporation of an additional Oligo-Ara-C molecule. (C) Volume size distribution (Size) and Z-potential (Zeta) of T22-GFP-H6 nanoparticles (top) and T22-GFP-H6-Ara-C NCs (bottom) measured by light scattering. Pdi indicates polydispersion index. Data is presented as mean ± SE. (D) Representative high-resolution images of electron microscopy (TEM and FESEM) of polydisperse well-formed nanoconstructs of T22-GFP-H6-Ara-C. Bars size: 20 nm. (E) Relative specific fluorescence of T22-GFP-H6 nanoparticles and T22-GFP-H6-Ara-C NCs measured at 510 nm upon excitation at 488 nm. (F) Confocal laser microscopy images of THP-1 cells upon exposure to 2 μM of T22-GFP-H6-Ara-C NCs for 24 h. Cell nuclei are labeled in blue, cell membranes are labeled in red and green signal correspond to T22-GFP-H6-Ara-C NCs fluorescence. Scale bars indicate 10 μm. SE, standard error. (For interpretation of the references to colour in this figure legend, the reader is referred to the Web version of this article.)

3.4. Pharmacokinetics and biodistribution of T22-GFP-H6-Ara-C in a CXCR4$^+$ AML mouse model

We evaluated the NC pharmacokinetics and biodistribution, after a single intravenous administration of 200 μg of T22-GFP-H6-Ara-C sacrificing the mice bearing SC tumors with THP-1 cells at different time points (10 min, 30 min, 2 h, 5 h, 24 h and 48 h) to measure the fluorescence emitted by the NC or its detection by WB with an anti-GFP antibody, in plasma, urine and different tissues.

The highest peak of T22-GFP-H6-Ara-C in plasma appeared 10 min

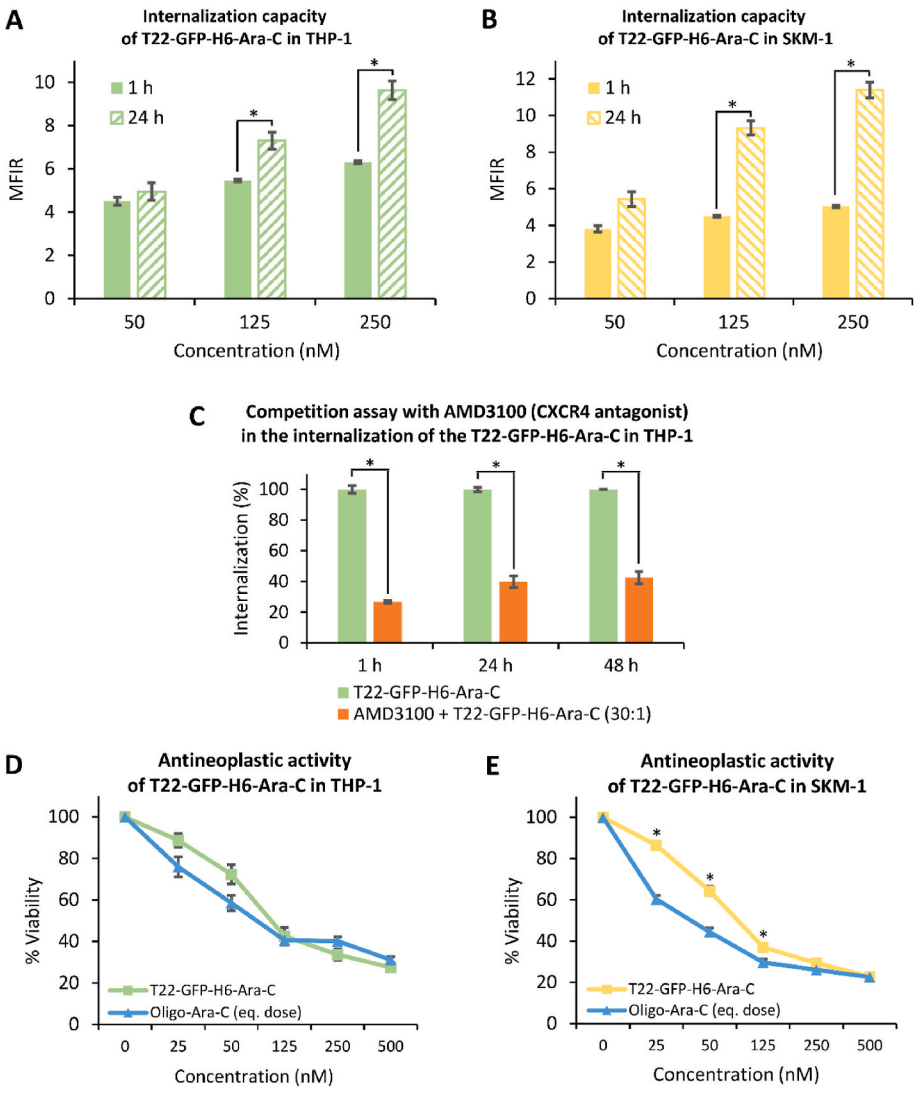

Fig. 2. Internalization and antineoplastic capacities of the T22-GFP-H6-Ara-C nanoparticle in CXCR4$^+$ AML cell lines. (A–B) Internalization capacity of T22-GFP-H6-Ara-C in THP-1 and SKM-1 at 1 and 24 h after exposure to different concentrations of the NC measured by flow cytometry. Results are presented by the mean fluorescence intensity (MFI) normalized by the MFI of buffer treated cells (MFI ratio or MFIR) ± SE. (C) Competition assay was performed by cytometry in THP-1 cells adding or not 7500 nM AMD3100 1 h prior to the administration of 250 nM T22-GFP-H6-Ara-C exposed for 1, 24 and 48 h (ratio 30:1). Results are presented by the mean percentage of internalization ± SE. (D–E) The antineoplastic activity was measured by XTT exposing THP-1 and SKM-1 to different concentrations of the T22-GFP-H6-Ara-C or the Oligo-Ara-C at equimolar doses incubated for 48 h. Results are presented by the mean percentage of viability ± SE. Mann-Whitney *U* test was used to test differences between groups indicated by * when *p*-value was <0.05. AML, Acute myeloid leukemia; MFIR, Mean fluorescence intensity ratio; SE, standard error.

after the intravenous injection of the NC ($1.82 \times 10^8 \pm 0.40 \times 10^8$) and decreased 7.3-times ($0.25 \times 10^8 \pm 0.07 \times 10^8$) at 30 min. Afterwards, the presence of NC in circulation was considerably reduced, 20-times at 2 h, 38.2-times at 5 h, 83.5-times at 24 h and, finally, almost undetectable levels were observed at 48 h (Fig. 3A and B). The levels of NC in plasma were very similar to the sum of the FLI detected in liver and kidneys at short times ($0.40 \times 10^8 \pm 0.09 \times 10^8$ and $1.56 \times 10^8 \pm 0.28 \times 10^8$ at 10 min and $0.09 \times 10^8 \pm 0.04 \times 10^8$ and $0.38 \times 10^8 \pm 0.08 \times 10^8$ at 30 min in liver and kidneys, respectively) (Fig. 3C and D). Moreover, by western blot, we observed the presence of the nanoparticle (anti-GFP staining) in plasma samples obtained from mice treated after 10 min with T22-GFP-H6-Ara-C and much lower NC expression at 30 min. In contrast, we did not observe any presence of T22-GFP-H6-Ara-C in urine samples at any time of the biodistribution study (Fig. 3E). Finally, the cumulative FLI quantification of T22-GFP-H6-Ara-C at longer times (2–48 h) showed a high amount of NC accumulation in SC tumor tissue ($2.67 \times 10^8 \pm 0.50 \times 10^8$), whereas much lower levels of NC were present at the non-tumor organs, such as liver ($0.54 \times 10^8 \pm 0.16 \times 10^8$), kidneys ($0.51 \times 10^8 \pm 0.16 \times 10^8$) or lungs ($0.55 \times 10^8 \pm 0.09 \times 10^8$) (Fig. 3F).

Thus, all these results suggest that the NC transiently accesses the fenestrated vessels in the liver and kidneys during a short time period, to return to the bloodstream, without penetrating the parenchyma or being excreted through the urine, since at longer times the NC is mainly located to SC tumor.

3.5. *T22-GFP-H6-Ara-C dose response study in a CXCR4$^+$ AML mouse model*

To evaluate the anticancer activity of T22-GFP-H6-Ara-C in vivo, a disseminated AML mouse model was generated by intravenous injection of CXCR4$^+$ THP-1-Luci cells, as reported [25]. Two days after the i.v. injection of THP-1-Luci cells, 10 daily doses of buffer ($NaCO_3H$ NaCl pH = 8) or T22-GFP-H6-Ara-C (5, 25, 100 and 200 μg) were i.v. administered in different groups of mice in order to choose the NC dose with the highest antineoplastic effect and the lowest systemic toxicity. The results showed that mice administered with 5 or 25 μg of T22-GFP-H6-Ara-C did not reduce the leukemia dissemination compared to buffer-treated mice. In contrast, we observed significant differences between mice treated with buffer and mice treated with 100 μg or 200 μg of T22-GFP-H6-Ara-C at day 13 (2.3-fold and 5.6-fold lower BLI, respectively). Indeed, 200 μg-T22-GFP-Ara-C-treated mice group was the only one which showed a significantly lower leukemic dissemination (lower BLI signal) already on day 8 and day 10 compared to buffer-treated mice (Fig. 4A and B).

Furthermore, none of the mice treated with T22-GFP-H6-Ara-C showed significant mouse weight reduction at the end of the AML dissemination follow-up compared to control mice. Exceptionally, at day

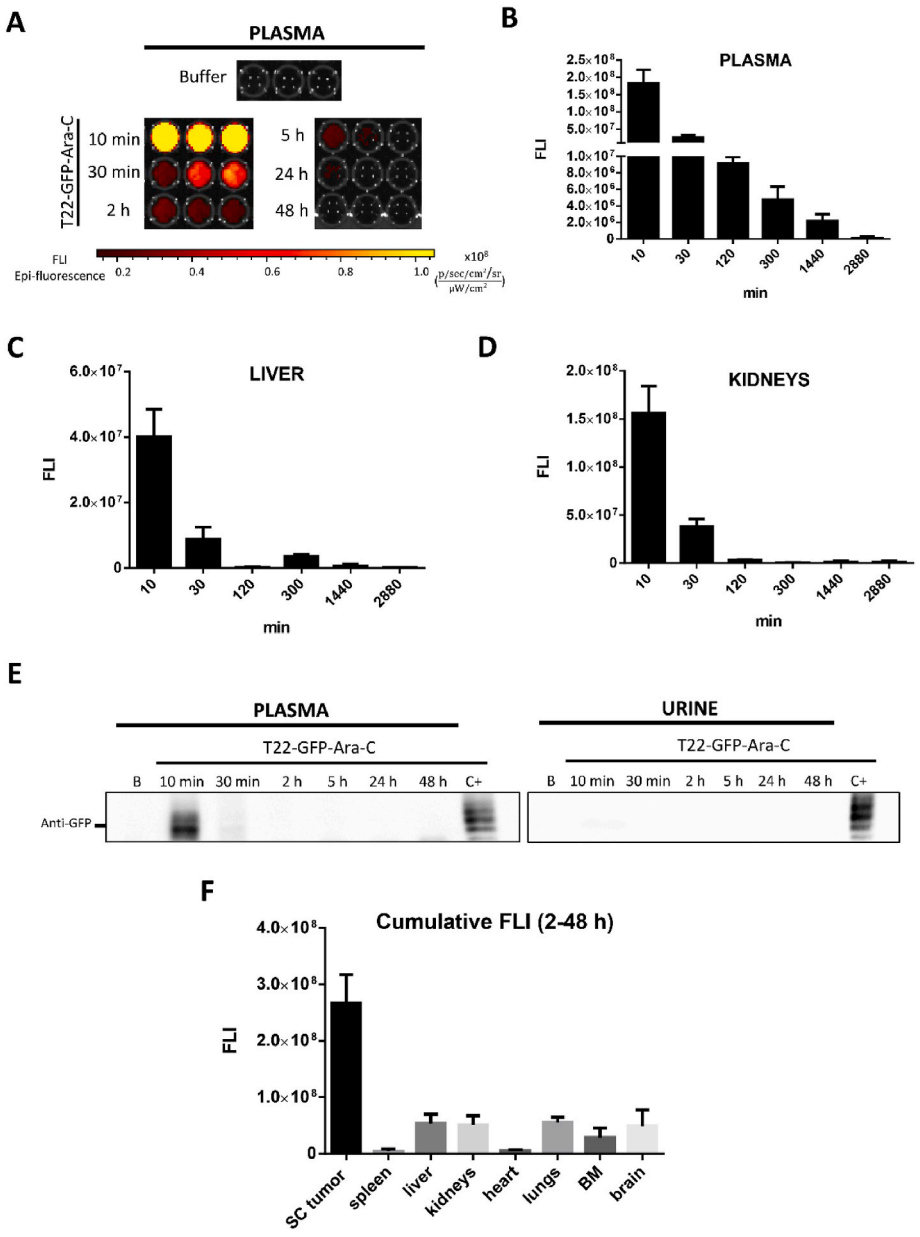

Fig. 3. Pharmacokinetics and biodistribution of T22-GFP-H6-Ara-C in a SC CXCR4$^+$ AML mouse model. (A) FLI images of 100 μL of plasma, acquired by IVIS Spectrum, from mice treated with a single dose of buffer ("Buffer", n = 3/group) or a single dose of 200 μg T22-GFP-H6-Ara-C ("T22-GFP-Ara-C") at 10 min, 30 min, 2 h, 5 h, 24 h and 48 h. (B) Plasma FLI quantification from buffer-treated mice (n = 3/group) and 200 μg NC-treated mice at different time points (10 min, 30 min, 2 h, 5 h, 24 h and 48 h, n = 3/group). (C–D) FLI quantification emitted by liver and kidneys ex vivo at different time points after the NC administration. (E) Western Blot analysis detecting the NC (anti-GFP staining) in plasma and urine samples collected from mice treated with buffer or NC at different time points. C+ is a positive control for GFP staining. (F) Cumulative FLI registered from mice treated with NC from 2 to 48 h in SC tumors and normal organs. Cumulative FLI were quantified using the area under the curve (AUC). FLI quantifications were performed subtracting the auto-fluorescence emitted from buffer samples or organs. B, buffer.

3 after cell injection, mice treated with 200 μg of T22-GFP-H6-Ara-C showed a significant loss of mouse weight, which was immediately restored (Fig. 4C). Moreover, the biochemical parameters determining hepatic (ALT and AST) and renal (creatinine) toxicity did not exhibit significant differences between control mice and mice treated with any concentration of T22-GFP-H6-Ara-C (Fig. 4D and E). Thus, the mice group treated with 200 μg of T22-GFP-H6-Ara-C demonstrated to have the highest antineoplastic effect without inducing neither loss of mouse weight nor hepatic or renal functional toxicity at the end of the experiment.

3.6. *Comparison of the antineoplastic effect of T22-GFP-H6-Ara-C and free Oligo-Ara-C in a CXCR4$^+$ AML mouse model*

Here, using the same design as the previous experiment, we evaluated the antineoplastic effect of the most effective T22-GFP-H6-Ara-C dosage (200 μg T22-GFP-H6-Ara-C for a total of 10 doses) and this effect was compared to that observed in mice treated with free Oligo-Ara-C at equimolar doses or administered with NC buffer. The weight of the mice treated with Oligo-Ara-C was significantly lower than buffer-treated mice from the third day and until the eighth day after the injection of cells (that is, during the first 7 doses). After that period, mouse weight between both groups was similar. In contrast, the weight of NC-treated mice was significantly lower than this in buffer-treated group only at the third day after cell injection, exactly the same event that occurred in the preliminary experiment. No differences in body weight were found between the Oligo-Ara-C and the T22-GFP-Ara-C-treated groups (Fig. S2B).

Disease progression was monitored, along the experiment, by analyzing the bioluminescence emitted (BLI) by each mouse with the IVIS spectrum system. Treatment with T22-GFP-H6-Ara-C decreased mice BLI compared to the buffer or Oligo-Ara-C-treated mice after the sixth dose (day 8) (Fig. 5A and B). In contrast, treatment with Oligo-Ara-C needed two additional doses to decrease disease progression (day 10). However, in a more global study of BLI along time, performed by analyzing the AUC of the different treatments, T22-GFP-H6-Ara-C treatment induced a significant blockade of AML progression by reducing the emitted luminescence a 75 ± 2% (9.8E+07 ± 2.6E+06 BLI

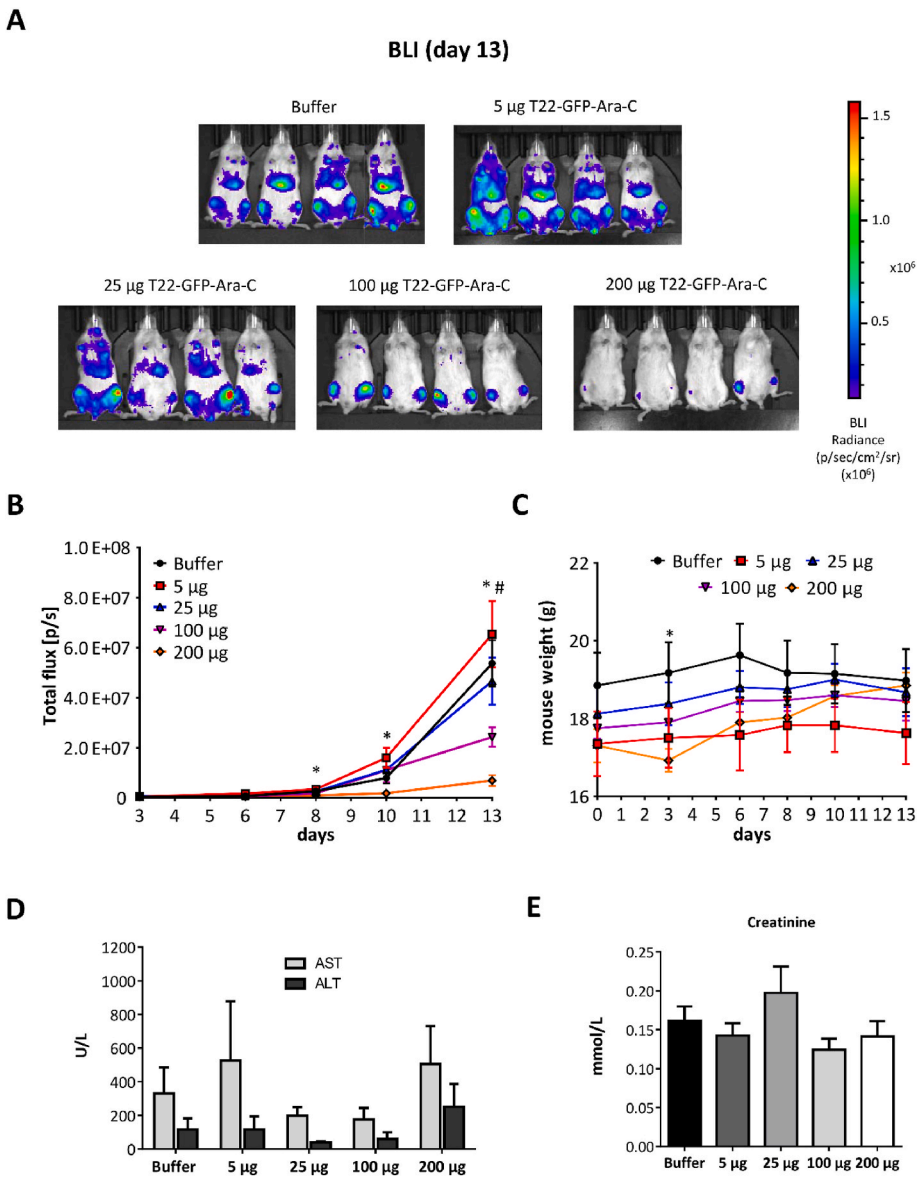

Fig. 4. T22-GFP-H6-Ara-C dose response study in a disseminated CXCR4^{+} AML mouse model. (A) BLI registered in mice treated with ten doses of NC buffer ("Buffer", n = 4) or ten doses of different T22-GFP-H6-Ara-C concentrations (5, 25, 100 and 200 μg, "T22-GFP-Ara-C", n = 4/group) at day 13 after the intravenous administration of THP1-Luci cells. (B) BLI quantification of mice treated with buffer or different T22-GFP-H6-Ara-C concentrations (5, 25, 100 and 200 μg) throughout the leukemia dissemination follow-up. Results are presented in total flux units [p/s]. (C) Mouse weight of buffer- or NC-treated-mice during the experiment. (D) Functional analysis measuring the levels of hepatic transaminases (AST and ALT) and (E) creatinine in mice treated with buffer or mice groups treated with different concentrations of T22-GFP-H6-Ara-C at the end of the experiment. * denotes statistical difference ($p < 0.05$) between buffer-treated mice and 200 μg-NC-treated mice. # denotes statistical difference ($p < 0.05$) between buffer-treated mice and 100 μg-NC-treated mice. Mann-Whitney *U* test was used to analyze differences between groups. All results are expressed as mean ± SE. BLI, bioluminescence; ALT, alanine aminotransferase; AST, aspartate aminotransferase; SE, standard error.

Total Flux reduction) compared to the buffer-treated group, whereas the Oligo-Ara-C treatment reached only a 21 ± 10% reduction (2.7E+07 ± 1.3E+07 BLI Total Flux) (Fig. 5C).

When the animals had signs of advanced disease, mice of all groups were euthanized and AML dissemination was studied locally in tissues by analyzing BLI ex vivo using the IVIS spectrum. In contrast to treatment with T22-GFP-H6-Ara-C that decreased significantly BLI levels in bone marrow tissues, including backbone, hindlimbs and cranium, Oligo-Ara-C treatment only significantly reduced BLI in cranium (Fig. 6A, B and C); however, this reduction was significantly lower than the exerted by the NC. In addition, BLI in spleen and liver was decreased significantly by both treatments, as compared to buffer-treated mice, however the reduction of AML cell dissemination in these organs was more pronounced in the NC-treated mice (Fig. 6D and E).

Finally, AML target tissues were analyzed by IHC to detect and quantify the area occupied by leukemic cells using the human CD45 marker. T22-GFP-H6-Ara-C treatment decreased significantly the dissemination of leukemic cells in liver, spleen, backbone and hindlimbs compared to that of the buffer-treated mice in a 71 ± 1, 99 ± 0, or 76 ± 3 and 61 ± 5%, respectively. In contrast, Oligo-Ara-C treatment only decreased significantly AML dissemination in spleen reaching a 74 ± 1% reduction of CD45 positive leukemic cells compared to buffer treatment (Fig. 7A and B). Moreover, the NC treatment reduced significantly leukemic dissemination in all tissues compared to the Oligo-Ara-C treatment, including the spleen.

3.7. Evaluation of toxicity in NC on-target and off-target mouse tissues

Finally, hematoxylin-eosin staining was performed to assess the possible toxicity of the different treatments in tissues. All analyzed samples showed a lack of relevant toxicity for the T22-GFP-H6-Ara-C or the Oligo-Ara-C treatment, compared to the buffer treatment, after a careful inspection of the possible occurrence of inflammatory processes, steatosis, hemorrhages or morphological changes in normal tissues (on-target NC toxicity) such as liver, spleen, backbone, or hindlimbs. Furthermore, the off-target tissues of experimental mice, such as lungs, kidneys or heart, did not show congestion, edema or intraalveolar hemorrhage, neither the glomerulus and surrounding renal tubules showed cytoplasmic vacuolation or eosinophilic protein accumulation nor the heart tissue had morphological alterations (Fig. 8).

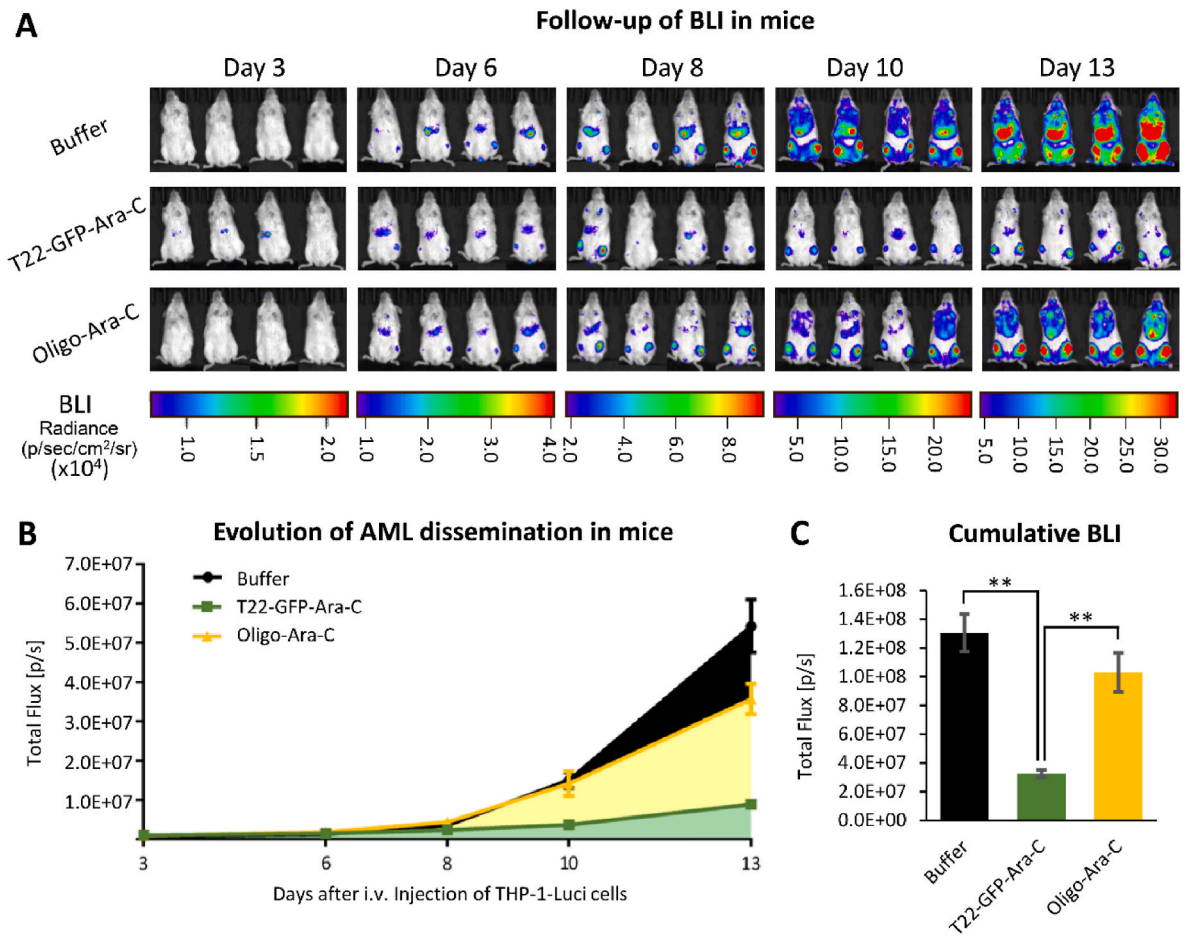

Fig. 5. Antineoplastic effect of T22-GFP-H6-Ara-C and free Oligo-Ara-C in a CXCR4$^+$ AML mouse model. (A) Follow-up of AML dissemination in NSG mice treated with buffer ($NaCO_3H$ + NaCl pH = 8) ("Buffer", n = 8), T22-GFP-H6-Ara-C ("T22-GFP-Ara-C", n = 8) or free Oligo-Ara-C (Oligo-Ara-C, n = 8) during treatment monitoring mice BLI in IVIS spectrum. (B) Evolution of AML dissemination of mice treated with buffer, T22-GFP-H6-Ara-C or Oligo-Ara-C measuring mice BLI by IVIS Spectrum. Results are presented by mean of total flux [p/s] ± SE. (C) Cumulative BLI of the different treated mouse groups during the treatment quantifying area under the curve of AML evolution for each mouse. Results are presented as mean of area under the curve in total flux units [p/s] ± SE. Mann-Whitney *U* test was used to analyze significant differences between groups, and they are indicated by ** when p-value was <0.01. AML, Acute myeloid leukemia; BLI, bioluminescence; i.v., intravenous; SE, standard error.

4. Discussion

We demonstrated that the novel T22-GFP-H6-Ara-C NC reaches a high therapeutic activity in an AML mouse model through selective blockade of CXCR4$^+$ leukemic cell dissemination, as compared to the free Oligo-Ara-C, in the absence of on-target or off-target toxicities. This high therapeutic window is triggered by the multivalency of the protein-nanocarrier together with the 5-fold increased drug payload delivered to target leukemic cells, that is achieved by the conjugation of a pentameric form of Ara-C. We believe that the conjugation strategy applied in our NC can be widely exploited because an ADC that uses the same chemical strategy (e.g.trastuzumab emtansine, "Kadcyla") was already approved by the FDA [26].

Furthermore, this novel therapy displays several advantages as compared to classical chemotherapy or to previously developed nanomedicines. First, as Ara-C (Cytarabine) has a short plasma half-life, extense hepatic metabolism and rapid renal elimination (within 24 h about 80% of the drug is excreted in the urine) [27], it must be administered as a continuous intravenous infusion to reach sustained and effective antineoplastic concentrations. Nevertheless, the prolonged exposure to high Ara-C concentrations triggers severe adverse effects that include bone marrow suppression, hepatic dysfunction or infectious complications [28,29]. In contrast, our results support a dramatic change in the pharmacokinetics and pharmacodynamics of the 13.4 nm T22-GFP-H6-Ara-C NC, as compared to free-Ara-C, since it avoids hepatic metabolism and renal excretion (cut-off 7 nm), leading to a high accumulation in CXCR4$^+$ cancer tissues, while evading its accumulation in normal tissues. This biodistribution change leads, in turn, to a potent antineoplastic effect of T22-GFP-H6-Ara-C specifically to CXCR4 overexpressing leukemic cells in the absence of toxicity that could significantly reduce the adverse effects of classical Ara-C-based AML therapy.

To support this argument, we report that T22-GFP-H6-Ara-C displays comparable physicochemical characteristics to the T22-GFP-H6 nanocarrier, which was our first protein nanoparticle displaying a well-characterized multivalent targeting approach. Here, we have demonstrated that the conjugation of the Oligo-Ara-C prodrug to T22-GFP-H6 does not affect the tertiary structure of the protein, its stability or its functionality neither its capacity to internalize in CXCR4$^+$ cells in vitro and in vivo [16,30]. Moreover, regarding its molecular mechanism of anticancer activity, once the NC specifically internalizes in target cancer cells, the molecules of Ara-C are sequentially released in the cytosol by the 3′ exonucleases that cleave the phosphodiester bond between sugars of the Oligo-Ara-C in the 3′ end to 5' direction [31]. Next, the released Ara-C is metabolized intracellularly into its active triphosphate form that acts as an antimetabolite by competing with cytidine for incorporation into DNA [27].

Because of its high therapeutic index in our disseminated AML mouse model, our NC could be indicated in more than a half of AML patients

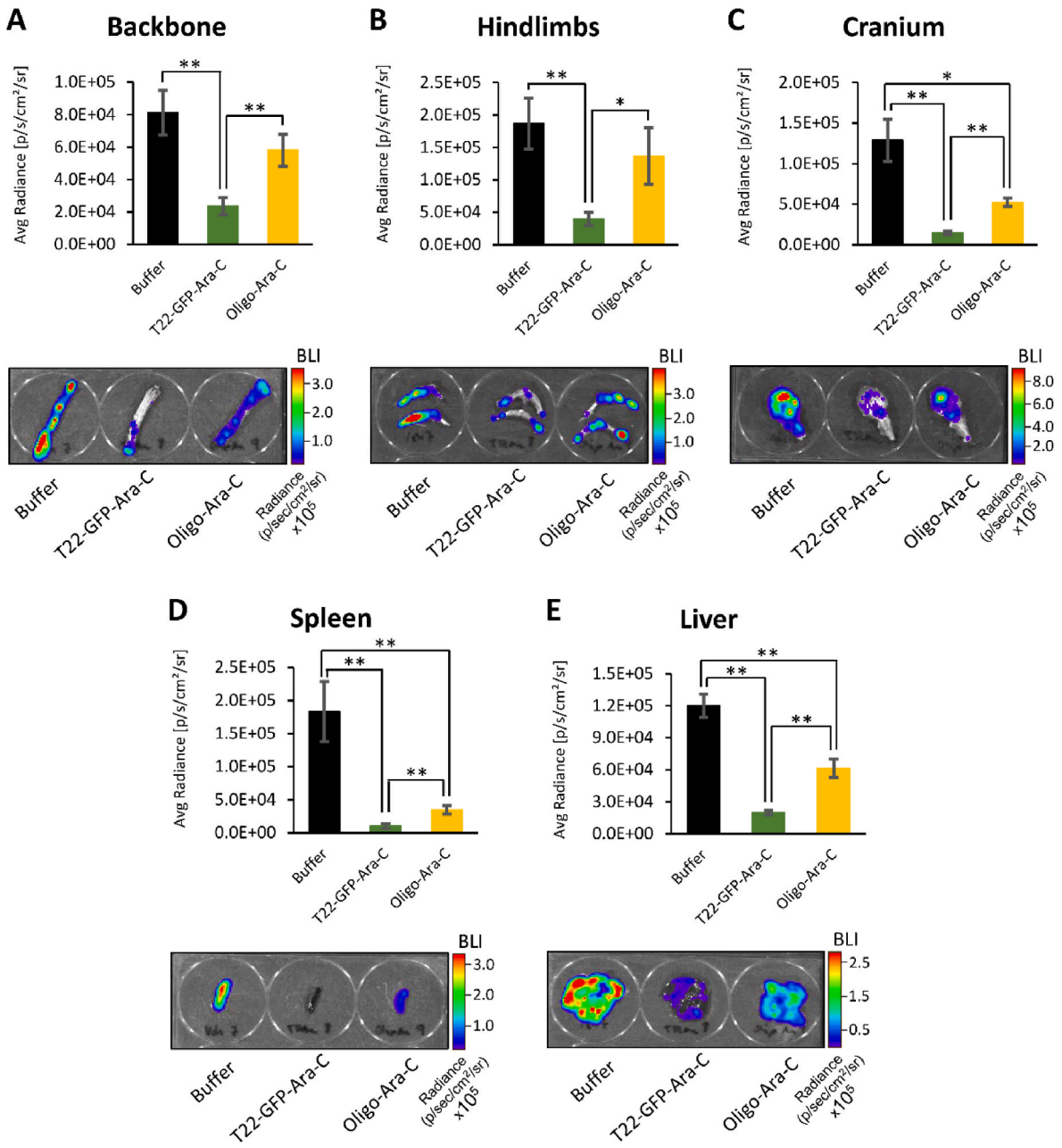

Fig. 6. Antineoplastic effect in CXCR4$^+$ AML affected organs ex vivo after mice treatment with T22-GFP-H6-Ara-C or Oligo-Ara-C. (A–E) Ex vivo BLI analysis of backbone, hindlimbs, cranium, spleen and liver of mice after treatment with buffer, T22-GFP-H6-Ara-C or Oligo-Ara-C. Graphs represent the quantitation of BLI presented as mean of average radiance ± SE for each tissue and representative images of these analyses show the BLI levels measured in IVIS Spectrum. * or ** indicate p-value <0.05 or <0.01, respectively, using Mann-Whitney *U* test to analyze significant differences between groups. AML, Acute myeloid leukemia; Avg, average; BLI, bioluminescence; SE, standard error.

that display CXCR4 overexpression in their leukemic cells, who currently lack clear therapeutic options. The AML patient subsets bearing CXCR4$^+$ leukemic cells, candidates to be treated with our NC, include patients with AML *de novo* (50–55%), which associate with poor prognosis and shorter disease-free survival; elderly (≥65 years) or co-morbid AML patients in whom intensive chemotherapy is not indicated, and AML patients scheduled for a second round of intensive chemotherapy or an invasive allogenic transplant, involving 50–70% of these that relapse after Ara-C based-therapy [1,2,17,18,18–22,32–35].

Most importantly, it is known that leukemic stem cells (LSCs) protection in the bone marrow niche is dependent on CXCR4 and its interaction with CXCL12 [24,36,37]. Accordingly, eliminating CXCR4$^+$ leukemic cells is considered a sound and effective strategy to eradicate the development of AML as a consequence of the reduction of LSCs homing and trafficking in the bone marrow [24,38–46]. In this work, T22-GFP-H6-Ara-C has a high cytotoxic effect against the THP-1 leukemic cell line that contains a large proportion of cells with high ALDH activity, a property directly linked to the LSC phenotype [47]. Thus, our NC displays a clear advantage over the current therapy because of its capacity of selectively targeting and ablating CXCR4$^+$ AML cells and consequently the LSCs.

Besides that, most nanoparticles being tested in clinical trials are untargeted [15,48,49]. For example, the CPX-351, a marketed liposome that encapsulates Ara-C and daunorubicin, changes only the drug pharmacokinetics, rather than proving preferential uptake by leukemia cells, as it is claimed. Thus, CPX-351 achieves low rate of clinical

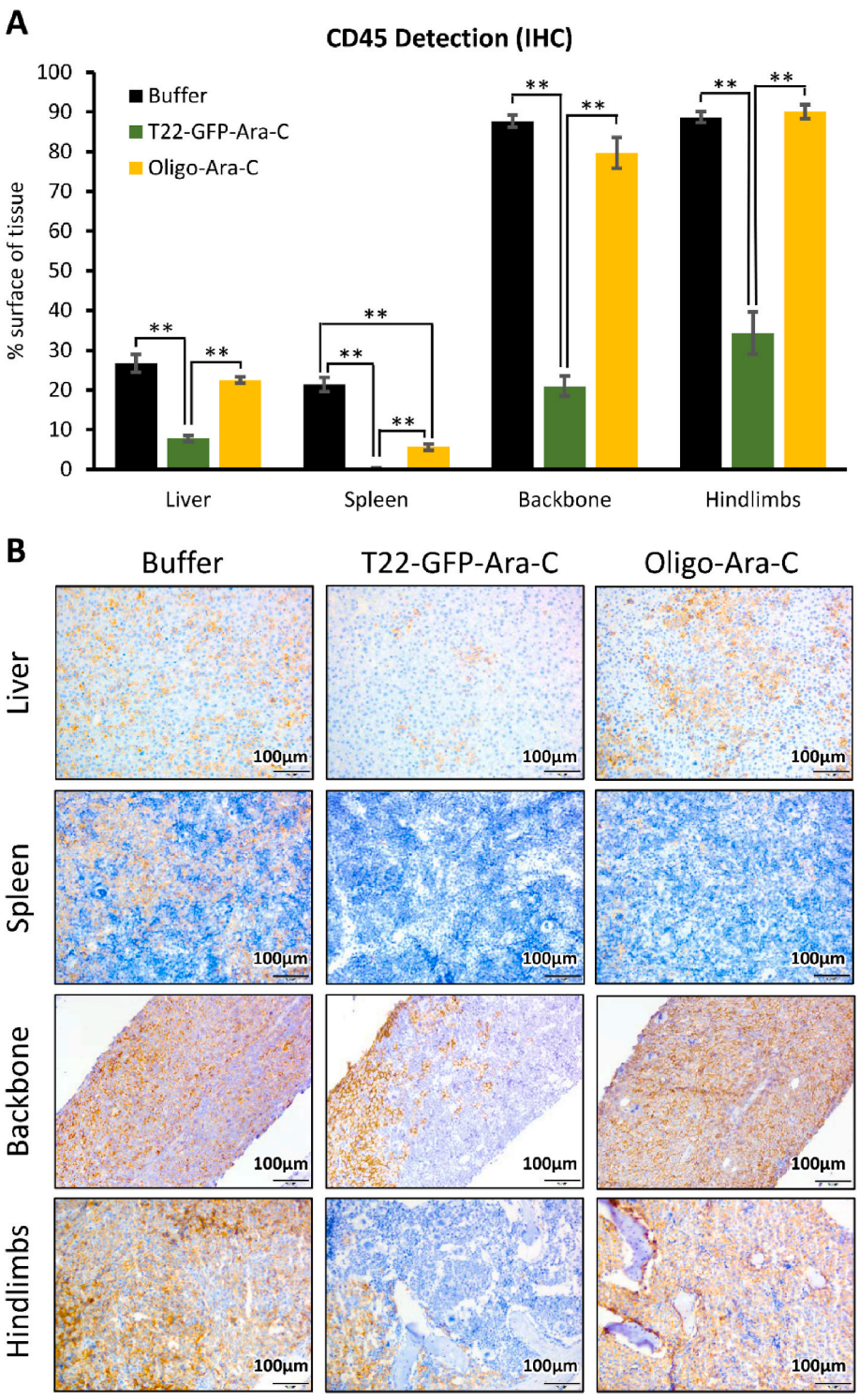

Fig. 7. Detection and quantitation of disseminated leukemic cells in tissues of T22-GFP-Ara-C or Oligo-Ara-C-treated mice. (A) Quantitation of leukemic cells in liver, spleen, backbone and hindlimbs performing human CD45 detection (marker of leukemic cells) by IHC in mice treated with buffer, T22-GFP-H6-Ara-C or Oligo-Ara-C. Results are presented as mean of surface percentage with CD45 positive cells ± SE. ** indicates significant differences between groups with a p-value <0.01 using Mann-Whitney *U* test. (B) Representative images of the CD45 detection by IHC in liver, spleen, backbone and hindlimbs according to the different treated mouse groups. IHC, immunohistochemistry; SE, standard error.

response in AML at high risk or relapsed-patients, showing similar toxicity to intensive chemotherapy, which has prompted its use in combination [50]. Similarly, additional untargeted nanomedicines include PLA/PLGA polymeric nanoparticles containing Aurora kinase B inhibitors, or liposomes encapsulating Annamycin or Grb2 antisense-encapsulated that need also to be used in combination with targeted drugs [51]. Thus, the preclinical trend is now to develop liposomes or polymeric nanoparticles that target relevant markers for AML (e.g., anti-CD33, anti-CD45 mAbs) [14]; however, once injected in the bloodstream they acquire a "protein corona" that limits their targeting capacity and stimulates their phagocytosis by the reticuloendothelial system [52,53]. In sharp contrast, our protein-based nanoparticles maintain their targeting capacity because their protein nature avoids corona formation [30,54].

Mainly, two T22-GFP-H6-Ara-C features determine the advantage of our nanotechnological approach as compared to other nanoparticle drugs. On the one hand, the multivalency of the NC, based on the incorporation of around 11 ligands that target the CXCR4 receptor in a single self-assembled nanoparticle, confers super-selectivity. This feature permits the interaction of the target receptor only when its

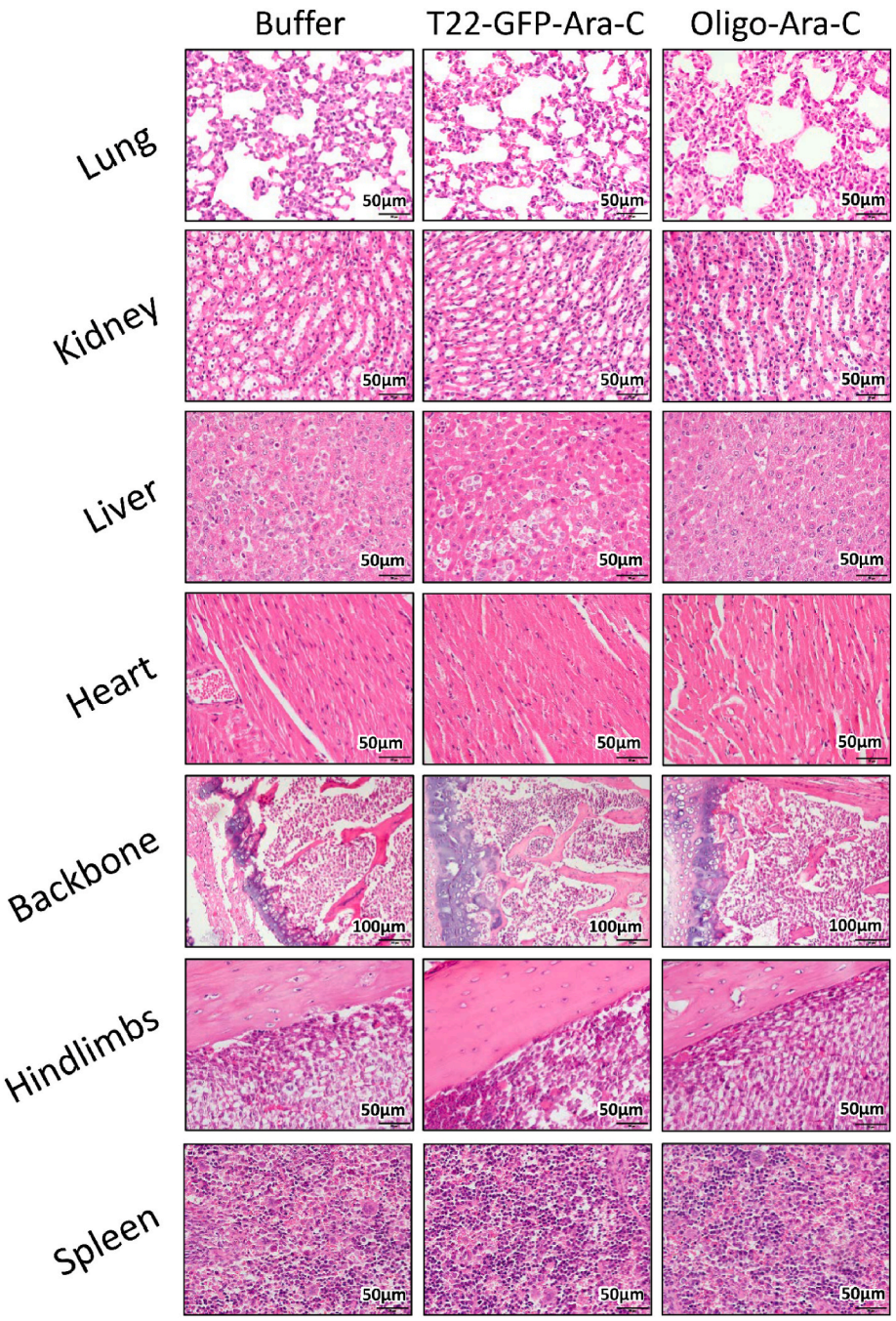

Fig. 8. Toxicity study in H&E stained tissue sections of mice treated with T22-GFP-H6-Ara-C or Oligo-Ara-C. Hematoxylin and eosin staining of target AML tissues such as liver, spleen, backbone and hindlimbs, and non-target AML tissues such as lung, kidney and heart of mice treated with buffer, T22-GFP-H6-Ara-C or Oligo-Ara-C.

density in the cell surface is higher than a specific threshold, showing an ON/OFF effect [55]. Therefore, T22-GFP-H6-Ara-C could only internalize in leukemic cells with high CXCR4 expression (e.g. LSCs) while avoiding internalization in normal cells, which display low CXCR4 expression [56]. This argument is supported by the fact that the T22-GFP-H6 nanocarrier achieves 86.0% accumulation in cancer tissues, as compared to untargeted nanoparticles that reach only an average of 0.7% of the administered dose accumulated in cancer tissues or the antibody-drug conjugates that reach only 0.1% [57,58]. On the other hand, our NC is able to incorporate a multimeric Oligo-Ara-C prodrug that allows to deliver a huge drug payload, which consequently achieves a high antineoplastic effect in target cells. Although we conjugated previously oligomeric drugs to protein nanoparticle [59,60], this is the first time that an oligomeric form of Ara-C is synthetized to be used as a prodrug.

Finally, as our study represents a prove-of-concept assay that demonstrates the high potential of T22-GFP-H6-Ara-C, we expect, in the near future, to replace the GFP scaffold protein in our NC by the recently engineered and structurally identical human counterpart (HSNBT) that is derived from the G2 domain of the human nidogen and, thus, avoids the immunogenicity that could be associated to the exogenous fluorescent protein [61].

5. Conclusion

In conclusion, we have generated a novel T22-GFP-H6-Ara-C

protein-based NC that highly enhances the therapeutic window of current drugs by combining nanoparticle multivalency, to achieve selective targeting CXCR4$^+$ cancer cells, with a multimeric prodrug to increase the conjugated payload drug. In addition, the T22-GFP-H6-Ara-C induction of negligible toxicity and higher antineoplastic effect observed in the disseminated CXCR4$^+$ AML mouse model, suggest their use as an alternative approach to non-intensive therapies in AML patients that show a low rate of complete remissions and still severe adverse effects.

Funding

This work was supported by Instituto de Salud Carlos III (ISCIII, Cofunding from FEDER) [PI18/00650, PIE15/00028, PI15/00378 and EU COST Action CA 17 140 to R.M.; FIS PI17/01246 and RD16/0011/0028 to J.S.; and PI20/00400 to U·U.]; Agencia Estatal de Investigación (AEI) and Fondo Europeo de Desarrollo Regional (FEDER) (grant BIO2016-76063-R, AEI/FEDER, UE) to A.V.; (grant PID2019-105416RB-I00) to E. V.; CIBER-BBN [CB06/01/1031 and 4NanoMets to R.M., VENOM4-CANCER to A.V., NANOREMOTE to E.V. and NANOLINK to U·U.]; AGAUR [2017 FI_B 00680 to A.F., 2018 FI_B2_00051 to L.S.G.; 2017-SGR-865 to R.M., 2017-SGR-1395 to J.S. and 2017SGR-229 to A.V.]; Josep Carreras Leukemia Research Institute [P/AG to R.M.]; La Marató TV3 [201 941-30-31-32 to J.S. and A.V.]; a grant from the Cellex Foundation, Barcelona [to J.S.]; a grant from La Generalitat de Catalunya (PERIS) [SLT002/16/00433to J.S.]; a grant from the Generalitat de Catalunya CERCA Programme. U.U. is supported by Miguel Servet fellowship (CP19/00028) from Instituto de Salud Carlos III co-funded by Fondo Social Europeo (ESF investing in your future). Finally, A.V. received an ICREA ACADEMIA Award supported by the Catalan Government.

We are also indebted to the ISCIII Networking Research Center on Bioengineering, Biomaterials and Nanomedicine (CIBER-BBN) and its ICTS Nanbiosis Platform for their funding. The bioluminescent follow-up of cancer cells and toxicity studies has been performed in the ICTS-141007 Nanbiosis Platform, using its CIBER-BBN Nanotoxicology Unit (http://www.nanbiosis.es/portfolio/u18-nanotoxicology-unit/). Protein production has been partially performed by the ICTS "NANBIOSIS", more specifically by the Protein Production Platform of CIBER-BBN/IBB (http://www.nanbiosis.es/unit/u1-protein-production-platform-ppp/). Finally, we are very grateful to Servei de Microscopia from UAB for their excellent confocal and electron microscopy services and especially to Alejandro Sánchez-Chardi for its excellent support and contribution in TEM and FESEM images.

Credit author statement

Conception and design: V.P., U.U., A.F., A.A., R.E., E.V., I.C. and R. M.; Development of Methodology: V.P., U.U., A.F., A.A., L.S.G., N.S., L. C., L.A.C. and P.A.; Acquisition of data: V.P., U.U., A.F., Y.N. and A.G.L. Histopathological analysis: V.P. and A.G.; Formal analysis and interpretation of data: V.P., U.U., A.F., J.S., A.V., E.V., I.C. and R.M.; Drafted the manuscript: V.P., U.U. and A.F.; Review and revision of manuscript: A.V., U.U., E.V., I.C. and R.M. Study supervision: E.V., I.C. and R.M.

Data availability

The raw/processed data required to reproduce these findings cannot be shared at this time due to legal or ethical reasons.

Declaration of competing interest

The authors declare the following financial interests/personal relationships which may be considered as potential competing interests: E. V., R.M. and A.V. are co-founders of Nanoligent, a company devoted to develop anticancer drugs based on proteins. U.U., E.V., A.V., R.M. and I. C. are cited as inventors in a patent application (EP11382005.4) covering the therapeutic use of T22. All other authors report no conflicts of interest in this work.

Appendix A. Supplementary data

Supplementary data to this article can be found online at https://doi.org/10.1016/j.biomaterials.2021.121258.

References

[1] H. Döhner, E. Estey, D. Grimwade, S. Amadori, F.R. Appelbaum, T. Büchner, H. Dombret, B.L. Ebert, P. Fenaux, R.A. Larson, R.L. Levine, F. Lo-Coco, T. Naoe, D. Niederwieser, G.J. Ossenkoppele, M. Sanz, J. Sierra, M.S. Tallman, H.-F. Tien, A. H. Wei, B. Löwenberg, C.D. Bloomfield, Diagnosis and management of AML in adults: 2017 ELN recommendations from an international expert panel, Blood 129 (2017) 424–447, https://doi.org/10.1182/blood-2016-08-733196.

[2] M. Heuser, Y. Ofran, N. Boissel, S. Brunet Mauri, C. Craddock, J. Janssen, A. Wierzbowska, C. Buske, Acute myeloid leukaemia in adult patients: ESMO Clinical Practice Guidelines for diagnosis, treatment and follow-up, Ann. Oncol. Off. J. Eur. Soc. Med. Oncol. 31 (2020) 697–712, https://doi.org/10.1016/j.annonc.2020.02.018.

[3] N.L. Crossnohere, D.R. Richardson, C. Reinhart, B. O'Donoghue, S.M. Love, B. D. Smith, J.F.P. Bridges, Side effects from acute myeloid leukemia treatment: results from a national survey, Curr. Med. Res. Opin. 35 (2019) 1965–1970, https://doi.org/10.1080/03007995.2019.1631149.

[4] S.A. Buckley, M. Othus, V. Vainstein, J.L. Abkowitz, E.H. Estey, R.B. Walter, Prediction of adverse events during intensive induction chemotherapy for acute myeloid leukemia or high-grade myelodysplastic syndromes, Am. J. Hematol. 89 (2014) 423–428, https://doi.org/10.1002/ajh.23661.

[5] M. Volkova, R. Russell, Anthracycline cardiotoxicity: prevalence, pathogenesis and treatment, Curr. Cardiol. Rev. 7 (2011) 214–220, https://doi.org/10.2174/157340311799960645.

[6] K.T.J. Chen, R. Gilabert-Oriol, M.B. Bally, A.W.Y. Leung, Recent treatment advances and the role of nanotechnology, combination products, and immunotherapy in changing the therapeutic landscape of acute myeloid leukemia, Pharm. Res. 36 (2019) 125, https://doi.org/10.1007/s11095-019-2654-z.

[7] N.J. Short, M. Konopleva, T.M. Kadia, G. Borthakur, F. Ravandi, C.D. DiNardo, N. Daver, Advances in the treatment of acute myeloid leukemia: new drugs and new challenges, Cancer Discov. 10 (2020) 506–525, https://doi.org/10.1158/2159-8290.CD-19-1011.

[8] E.S. Winer, R.M. Stone, Novel therapy in Acute myeloid leukemia (AML): moving toward targeted approaches, Ther. Adv. Hematol. 10 (2019), https://doi.org/10.1177/2040620719860645, 2040620719860645.

[9] S.R. Bohl, L. Bullinger, F.G. Rücker, New targeted agents in acute myeloid leukemia: new hope on the rise, Int. J. Mol. Sci. 20 (2019), https://doi.org/10.3390/ijms20081983.

[10] A.L. Harris, C. Potter, C. Bunch, J. Boutagy, D.J. Harvey, D.G. Grahame-Smith, Pharmacokinetics of cytosine arabinoside in patients with acute myeloid leukaemia, Br. J. Clin. Pharmacol. 8 (1979) 219–227, https://doi.org/10.1111/j.1365-2125.1979.tb01005.x.

[11] J. Robert, L. Gianni, Pharmacokinetics and metabolism of anthracyclines, Cancer Surv. 17 (1993) 219–252.

[12] H.-P. Gerber, P.D. Senter, I.S. Grewal, Antibody drug-conjugates targeting the tumor vasculature: current and future developments, mAbs 1 (2009) 247–253, https://doi.org/10.4161/mabs.1.3.8515.

[13] R.X. Zhang, J. Li, T. Zhang, M.A. Amini, C. He, B. Lu, T. Ahmed, H. Lip, A.M. Rauth, X.Y. Wu, Importance of integrating nanotechnology with pharmacology and physiology for innovative drug delivery and therapy – an illustration with firsthand examples, Acta Pharmacol. Sin. 39 (2018) 825–844, https://doi.org/10.1038/aps.2018.33.

[14] X. Huang, H. Lin, F. Huang, Y. Xie, K.H. Wong, X. Chen, D. Wu, A. Lu, Z. Yang, Targeting approaches of nanomedicines in acute myeloid leukemia, Dose-Response 17 (2019), https://doi.org/10.1177/1559325819887048, 1559325819887048.

[15] F. Sauvage, G. Barratt, L. Herfindal, J. Vergnaud-Gauduchon, The use of nanocarriers in acute myeloid leukaemia therapy: challenges and current status, Curr. Pharmaceut. Biotechnol. 17 (2016) 30–41, https://doi.org/10.2174/1389201016666150817095045.

[16] U. Unzueta, M.V. Céspedes, N. Ferrer-Miralles, I. Casanova, J. Cedano, J. L. Corchero, J. Domingo-Espín, A. Villaverde, R. Mangues, E. Vázquez, Intracellular CXCR4$^+$ cell targeting with T22-empowered protein-only nanoparticles, Int. J. Nanomed. 7 (2012) 4533–4544, https://doi.org/10.2147/IJN.S34450.

[17] W. Du, C. Lu, X. Zhu, D. Hu, X. Chen, J. Li, W. Liu, J. Zhu, Y. He, J. Yao, Prognostic significance of CXCR4 expression in acute myeloid leukemia, Cancer Med. 8 (2019) 6595–6603, https://doi.org/10.1002/cam4.2535.

[18] T. Cao, Y. Ye, H. Liao, X. Shuai, Y. Jin, J. Su, Q. Zheng, Relationship between CXC chemokine receptor 4 expression and prognostic significance in acute myeloid leukemia, Medicine (Baltim.) (2019) 98, https://doi.org/10.1097/MD.0000000000015948.

[19] A.C. Spoo, M. Lübbert, W.G. Wierda, J.A. Burger, CXCR4 is a prognostic marker in acute myelogenous leukemia, Blood 109 (2007) 786–791, https://doi.org/10.1182/blood-2006-05-024844.

[20] J.Y. Ahn, K. Seo, O.K. Weinberg, D.A. Arber, The prognostic value of CXCR4 in acute myeloid leukemia, Appl. Immunohistochem. Mol. Morphol. AIMM 21 (2013) 79–84, https://doi.org/10.1097/PAI.0b013e3182606f4d.

[21] S. Konoplev, P. Lin, C.C. Yin, E. Lin, G.M.N. González, H.M. Kantarjian, M. Andreeff, L.J. Medeiros, M. Konopleva, CXCR4 expression, CXCR4 activation, and wild type NPM1 are independently associated with unfavorable prognosis in patients with acute myeloid leukemia, Clin. Lymphoma, Myeloma & Leukemia 13 (2013) 686–692, https://doi.org/10.1016/j.clml.2013.05.013.

[22] S. Konoplev, G.Z. Rassidakis, E. Estey, H. Kantarjian, C.I. Liakou, X. Huang, L. Xiao, M. Andreeff, M. Konopleva, L.J. Medeiros, Overexpression of CXCR4 predicts adverse overall and event-free survival in patients with unmutated FLT3 acute myeloid leukemia with normal karyotype, Cancer 109 (2007) 1152–1156, https://doi.org/10.1002/cncr.22510.

[23] A. Peled, S. Tavor, Role of CXCR4 in the pathogenesis of acute myeloid leukemia, Theranostics 3 (2013) 34–39, https://doi.org/10.7150/thno.5150.

[24] Z. Yazdani, Z. Mousavi, A. Moradabadi, G. Hassanshahi, Significance of CXCL12/CXCR4 ligand/receptor Axis in various aspects of acute myeloid leukemia, Cancer Manag. Res. 12 (2020) 2155–2165, https://doi.org/10.2147/CMAR.S234883.

[25] V. Pallarès, U. Unzueta, A. Falgàs, L. Sánchez-García, N. Serna, A. Gallardo, G. A. Morris, L. Alba-Castellón, P. Álamo, J. Sierra, A. Villaverde, E. Vázquez, I. Casanova, R. Mangues, An Auristatin nanoconjugate targeting CXCR4+ leukemic cells blocks acute myeloid leukemia dissemination, J. Hematol. Oncol.J Hematol Oncol. 13 (2020) 36, https://doi.org/10.1186/s13045-020-00863-9.

[26] M.T. Kim, Y. Chen, J. Marhoul, F. Jacobson, Statistical modeling of the drug load distribution on trastuzumab emtansine (Kadcyla), a lysine-linked antibody drug conjugate, Bioconjugate Chem. 25 (2014) 1223–1232, https://doi.org/10.1021/bc5000109.

[27] R. Di Francia, S. Crisci, A. De Monaco, C. Cafiero, A. Re, G. Iaccarino, R. De Filippi, F. Frigeri, G. Corazzelli, A. Micera, A. Pinto, Response and toxicity to cytarabine therapy in leukemia and lymphoma: from dose puzzle to pharmacogenomic biomarkers, Cancers 13 (2021) 966, https://doi.org/10.3390/cancers13050966.

[28] A. Hamada, T. Kawaguchi, M. Nakano, Clinical pharmacokinetics of cytarabine formulations, Clin. Pharmacokinet. 41 (2002) 705–718, https://doi.org/10.2165/00003088-200241100-00002.

[29] E. Cros, L. Jordheim, C. Dumontet, C.M. Galmarini, Problems related to resistance to cytarabine in acute myeloid leukemia, Leuk. Lymphoma 45 (2004) 1123–1132, https://doi.org/10.1080/1042819032000159861.

[30] A. Falgàs, V. Pallarès, U. Unzueta, M.V. Céspedes, I. Arroyo-Solera, M.J. Moreno, J. Sierra, A. Gallardo, M.A. Mangues, E. Vázquez, A. Villaverde, R. Mangues, I. Casanova, A CXCR4-targeted nanocarrier achieves highly selective tumor uptake in diffuse large B-cell lymphoma mouse models, Haematologica 105 (2020) 741–753, https://doi.org/10.3324/haematol.2018.211490.

[31] T. Nishino, K. Morikawa, Structure and function of nucleases in DNA repair: shape, grip and blade of the DNA scissors, Oncogene 21 (2002) 9022–9032, https://doi.org/10.1038/sj.onc.1206135.

[32] E.J.C. Rombouts, B. Pavic, B. Löwenberg, R.E. Ploemacher, Relation between CXCR-4 expression, Flt3 mutations, and unfavorable prognosis of adult acute myeloid leukemia, Blood 104 (2004) 550–557, https://doi.org/10.1182/blood-2004-02-0566.

[33] E. Tavernier-Tardy, J. Cornillon, L. Campos, P. Flandrin, A. Duval, N. Nadal, D. Guyotat, Prognostic value of CXCR4 and FAK expression in acute myelogenous leukemia, Leuk. Res. 33 (2009) 764–768, https://doi.org/10.1016/j.leukres.2008.10.014.

[34] J.A. Burger, CXCR4 in acute myelogenous leukemia (AML): when too much attraction is bad for you, Leuk. Res. 33 (2009) 747–748, https://doi.org/10.1016/j.leukres.2008.11.007.

[35] A.S. Rady, R.H. Badawy, B.M.E. Gamal, A.D. Darwish, R.S.A. Aziz, M.E. Gammal, R.A. Goweda, Association of CXCR4 expression and clinical outcome in different subsets of de novo acute myeloid leukemia patients, Clin. Lab. 66 (2020), https://doi.org/10.7754/Clin.Lab.2019.190725.

[36] J.A. Burger, A. Peled, CXCR4 antagonists: targeting the microenvironment in leukemia and other cancers, Leukemia 23 (2009) 43–52, https://doi.org/10.1038/leu.2008.299.

[37] J.A. Burger, A. Spoo, A. Dwenger, M. Burger, D. Behringer, CXCR4 chemokine receptors (CD184) and alpha4beta1 integrins mediate spontaneous migration of human CD34+ progenitors and acute myeloid leukaemia cells beneath marrow stromal cells (pseudoemperipolesis), Br. J. Haematol. 122 (2003) 579–589, https://doi.org/10.1046/j.1365-2141.2003.04466.x.

[38] R. Ramakrishnan, P. Peña-Martínez, P. Agarwal, M. Rodriguez-Zabala, M. Chapellier, C. Högberg, M. Eriksson, D. Yudovich, M. Shah, M. Ehinger, B. Nilsson, J. Larsson, A. Hagström-Andersson, B.L. Ebert, R. Bhatia, M. Järås, CXCR4 signaling has a CXCL12-independent essential role in murine MLL-AF9-driven acute myeloid leukemia, Cell Rep. 31 (2020) 107684, https://doi.org/10.1016/j.celrep.2020.107684.

[39] L. Behrmann, J. Wellbrock, W. Fiedler, Acute myeloid leukemia and the bone marrow niche—take a closer look, Front. Oncol. 8 (2018), https://doi.org/10.3389/fonc.2018.00444.

[40] Z. Zeng, Y.X. Shi, I.J. Samudio, R.-Y. Wang, X. Ling, O. Frolova, M. Levis, J. B. Rubin, R.R. Negrin, E.H. Estey, S. Konoplev, M. Andreeff, M. Konopleva, Targeting the leukemia microenvironment by CXCR4 inhibition overcomes resistance to kinase inhibitors and chemotherapy in AML, Blood 113 (2009) 6215–6224, https://doi.org/10.1182/blood-2008-05-158311.

[41] B. Nervi, P. Ramirez, M.P. Rettig, G.L. Uy, M.S. Holt, J.K. Ritchey, J.L. Prior, D. Piwnica-Worms, G. Bridger, T.J. Ley, J.F. DiPersio, Chemosensitization of acute myeloid leukemia (AML) following mobilization by the CXCR4 antagonist AMD3100, Blood 113 (2009) 6206–6214, https://doi.org/10.1182/blood-2008-06-162123.

[42] S. Tavor, I. Petit, S. Porozov, A. Avigdor, A. Dar, L. Leider-Trejo, N. Shemtov, V. Deutsch, E. Naparstek, A. Nagler, T. Lapidot, CXCR4 regulates migration and development of human acute myelogenous leukemia stem cells in transplanted NOD/SCID mice, Cancer Res. 64 (2004) 2817–2824, https://doi.org/10.1158/0008-5472.can-03-3693.

[43] C. Voermans, W.P.M. van Heese, I. de Jong, W.R. Gerritsen, C.E. van Der Schoot, Migratory behavior of leukemic cells from acute myeloid leukemia patients, Leukemia 16 (2002) 650–657, https://doi.org/10.1038/sj.leu.2402431.

[44] R. Möhle, F. Bautz, S. Rafii, M.A. Moore, W. Brugger, L. Kanz, The chemokine receptor CXCR-4 is expressed on CD34+ hematopoietic progenitors and leukemic cells and mediates transendothelial migration induced by stromal cell-derived factor-1, Blood 91 (1998) 4523–4530.

[45] S. Tavor, M. Eisenbach, J. Jacob-Hirsch, T. Golan, I. Petit, K. Benzion, S. Kay, S. Baron, N. Amariglio, V. Deutsch, E. Naparstek, G. Rechavi, The CXCR4 antagonist AMD3100 impairs survival of human AML cells and induces their differentiation, Leukemia 22 (2008) 2151–5158, https://doi.org/10.1038/leu.2008.238.

[46] E.A.R. Sison, E. McIntyre, D. Magoon, P. Brown, Dynamic chemotherapy-induced upregulation of CXCR4 expression: a mechanism of therapeutic resistance in pediatric AML, Mol. Cancer Res. MCR. 11 (2013) 1004–1016, https://doi.org/10.1158/1541-7786.MCR-13-0114.

[47] M.T. Lira Benício, P.S. Scheucher, A.B. Garcia, R.P. Falcao, E.M. Rego, Characterization of leukemic stem cells in AML cell lines using ALDH staining, Blood 122 (2013) 5409, https://doi.org/10.1182/blood.V122.21.5409.5409.

[48] B.S. Chhikara, K. Parang, Development of cytarabine prodrugs and delivery systems for leukemia treatment, Expet Opin. Drug Deliv. 7 (2010) 1399–1414, https://doi.org/10.1517/17425247.2010.527330.

[49] L. Brannon-Peppas, J.O. Blanchette, Nanoparticle and targeted systems for cancer therapy, Adv. Drug Deliv. Rev. 56 (2004) 1649–1659, https://doi.org/10.1016/j.addr.2004.02.014.

[50] L.D. Mayer, P. Tardi, A.C. Louie, CPX-351: a nanoscale liposomal co-formulation of daunorubicin and cytarabine with unique biodistribution and tumor cell uptake properties, Int. J. Nanomed. 14 (2019) 3819–3830, https://doi.org/10.2147/IJN.S139450.

[51] M. Houshmand, F. Garello, P. Circosta, R. Stefania, S. Aime, G. Saglio, C. Giachino, Nanocarriers as magic bullets in the treatment of leukemia, Nanomaterials 10 (2020), https://doi.org/10.3390/nano10020276.

[52] W. Lohcharoenkal, L. Wang, Y.C. Chen, Y. Rojanasakul, Protein nanoparticles as drug delivery carriers for cancer therapy, BioMed Res. Int. 2014 (2014), e180549, https://doi.org/10.1155/2014/180549.

[53] G.T. Noble, J.F. Stefanick, J.D. Ashley, T. Kiziltepe, B. Bilgicer, Ligand-targeted liposome design: challenges and fundamental considerations, Trends Biotechnol. 32 (2014) 32–45, https://doi.org/10.1016/j.tibtech.2013.09.007.

[54] M.V. Céspedes, U. Unzueta, P. Álamo, A. Gallardo, R. Sala, I. Casanova, M. A. Pavón, M.A. Mangues, M. Trías, A. López-Pousa, A. Villaverde, E. Vázquez, R. Mangues, Cancer-specific uptake of a liganded protein nanocarrier targeting aggressive CXCR4+ colorectal cancer models, Nanomed. Nanotechnol. Biol. Med. 12 (2016) 1987–1996, https://doi.org/10.1016/j.nano.2016.04.003.

[55] F.J. Martinez-Veracoechea, D. Frenkel, Designing super selectivity in multivalent nano-particle binding, Proc. Natl. Acad. Sci. Unit. States Am. 108 (2011) 10963–10968, https://doi.org/10.1073/pnas.1105351108.

[56] M. Liu, A. Apriceno, M. Sipin, E. Scarpa, L. Rodriguez-Arco, A. Poma, G. Marchello, G. Battaglia, S. Angioletti-Uberti, Combinatorial entropy behaviour leads to range selective binding in ligand-receptor interactions, Nat. Commun. 11 (2020) 4836, https://doi.org/10.1038/s41467-020-18603-5.

[57] S. Wilhelm, A.J. Tavares, Q. Dai, S. Ohta, J. Audet, H.F. Dvorak, W.C.W. Chan, Analysis of nanoparticle delivery to tumours, Nat. Rev. Mater. 1 (2016) 1–12, https://doi.org/10.1038/natrevmats.2016.14.

[58] J.M. Lambert, Antibody-drug conjugates (ADCs): magic bullets at last, Mol. Pharm. 12 (2015) 1701–1702, https://doi.org/10.1021/acs.molpharmaceut.5b00302.

[59] A. Aviñó, U. Unzueta, M. VirtudesCéspedes, I. Casanova, E. Vázquez, A. Villaverde, R. Mangues, R. Eritja, Efficient bioactive oligonucleotide-protein conjugation for cell-targeted cancer therapy, ChemistryOpen 8 (2019) 382–387, https://doi.org/10.1002/open.201900038.

[60] M.V. Céspedes, U. Unzueta, A. Aviñó, A. Gallardo, P. Álamo, R. Sala, A. Sánchez-Chardi, I. Casanova, M.A. Mangues, A. Lopez-Pousa, R. Eritja, A. Villaverde, E. Vázquez, R. Mangues, Selective depletion of metastatic stem cells as therapy for human colorectal cancer, EMBO Mol. Med. 10 (2018), https://doi.org/10.15252/emmm.201708772.

[61] P. Álamo, J. Cedano, O. Conchillo-Sole, O. Cano-Garrido, L. Alba-Castellon, N. Serna, A. Aviñó, L.M. Carrasco-Diaz, A. Sánchez-Chardi, C. Martinez-Torró, A. Gallardo, M. Cano, R. Eritja, A. Villaverde, R. Mangues, E. Vazquez, U. Unzueta, Rational engineering of a human GFP-like protein scaffold for humanized targeted nanomedicines, Acta Biomater. 130 (2021) 211–222, https://doi.org/10.1016/j.actbio.2021.06.001.